ABERRATIONS: THEIR EFFECT ON OFF-AXIS BEAM STEERING

THESIS

Christina N. Walton
Second Lieutenant, USAF

AFIT/GEP/ENP/87D - 10

DEPARTMENT OF THE AIR FORCE
AIR UNIVERSITY
AIR FORCE INSTITUTE OF TECHNOLOGY

Wright-Patterson Air Force Base, Ohio

AFIT/GEP/ENP/87D - 10

ABERRATIONS:
THEIR EFFECT ON OFF-AXIS BEAM STEERING

THESIS

Christina N. Walton
Second Lieutenant, USAF

AFIT/GEP/ENP/87D - 10

Approved for public release; distribution unlimited

AFIT/GEP/ENP/87D - 10

ABERRATIONS: THEIR EFFECT ON OFF-AXIS BEAM STEERING

THESIS

Presented to the Faculty of the School of Engineering

of the Air Force Institute of Technology

Air University

In Partial Fulfillment of the

Requirements for the Degrees of

Master of Science in Electrical Engineering

and

Master of Science in Engineering Physics

Christina N. Walton, B.S.

Second Lieutenant, USAF

December 1987

Preface

The purpose of the thesis was to qualitatively describe the effects of aberrations on off-axis beam steering for multi-aperture systems. A new expression analogous to Goodman's thin lens was developed which shows the beam degradation that occurs at angles, with respect to the optic axis, much greater than five degrees for a thin lens, and two degrees for a thick lens. It is my hope that this thesis will be the first in a series which will not only prove and validate the idea of phased optical beam steering, but to make an engineering analysis on such a system.

The analysis described in this research is of special interest to organizations such as SDI since it defines regions and specifications for a multi-aperture system which will not work. Hopefully with this research, a reliable system can be made to achieve the goals of SDI.

I would like to thank my advisor, LtCol Jim Mills, who has spent many an hour discussing this project with me. I would also like to especially thank Maj. Jim Lupo (user friendly) for his invaluable support, as confidante, and computer expert - without whom I am sure there would have been a baseball bat through more than one terminal. I would like to thank my parents, who happened to be stationed here three days after I did - please don't follow me to my next assignment! Its awful hard to have a daughter around for the first time in five years, and to refrain from calling because of thesis. And most importantly, I can never thank these two people so that they will ever understand. To the person who

stood by me to help me finish this thesis - even to staying up all night with me the night before it was due. May our future together be as beautiful as our past. And to my bestest friend and teddy bear, I can only hope that I helped you as much as you helped me as we went through this.

Christina N. Walton

Table of Contents

List of Figures

List of Tables

Abstract

The effect of aberrations on off-axis beam steering for multi-aperture systems was qualitatively investigated. A new expression analogous to Goodman's Thin Lens is proposed which shows the beam degradation that occurs at angles, with respect to the optic axis, much greater than five degrees for a thin lens, and two degrees for a thick lens. This expression was then applied to three multi-aperture configurations as a way to correctly predict the field-of-view for various optical systems. Analytical predictions supported by computational and experimental results are included. Although the beam degradation as the field-of-view or field angle is increased has a dramatic effect on the image quality, the power loss as the field angle is increased will be the major factor in designing a system of this type.

Aberrations: Their Effect On Off-Axis Beam Steering

I. Introduction

I.1. Problem Statement

In this thesis, the effect of aberrations on off-axis beam steering for multi-aperture systems was qualitatively investigated. A new expression analogous to Goodman's thin lens (1:80) is proposed which shows the beam degradation that occurs at angles, with respect to the optic axis, much greater than five degrees for a thin lens, and two degrees for a thick lens. This expression was then applied to three multi-aperture configurations as a way to correctly predict the field-of-view for various optical systems. This thesis includes analytical predictions supported by computational and experimental results.

I.2. Air Force Applications

Today a single phased array radar can do what previously might have required a battery of mechanically steered dishes. Phased array radars are a series of point emitters which radiate at microwave frequencies. If a phase shift is introduced at each emitter, then the beam can be steered as opposed to rotating a platform (or radar dish). The replacement of a single, movable antenna with an immobile array of radiating elements can offer more advantages than just electronic steering, reliability being one of them. A fixed array does not depend on fallible mechanical components such as bearings and motors. With increasing

simplicity and compactness, concomitant reductions in weight and increases in reliability, phased array radars can be deployed in space within a few years (2:94-102).

The President's Strategic Defense Initiative (SDI) has been proposed as the central defense concept in our nation for the years to come. One of the SDI missions, midcourse discrimination, requires simultaneous acquisition, identification, and tracking of a large number of targets over a twenty degree field-of-view. The obvious benefits of a phased array multi-aperture optical system, therefore, become very important to the Air Force and the Department of Defense.

The ability to achieve a large field-of-view from a multi-aperture optical system has been doubted by many based on the transfer function for a thin lens derived by Goodman (1:77-80). Based on the new expression derived to include the effects of off-axis radiation, beam steering for an uncorrected multi-aperture optical system is not realizable.

I.3. Background

The transmission function for a thin lens is given by Goodman (1:80) as:

$$t_l(x,y)=\exp\left[\frac{-jk}{2f}(x^2+y^2)\right] \tag{1.1}$$

The expression was derived to enable diffraction analysis for on-axis radiation. This function was used to show how a lens can perform the Fourier transform of an input.

Geary and Peterson (3:52-54) derived a new transfer function for a thin lens which included one more term, from the binomial expansion, that had been assumed negligible in Goodman's expression. They showed that this extra term included the effects of spherical aberration. However, if the rest of the terms are kept in the expression for the transfer function, no further information is gained about the other third order aberrations such as astigmatism, coma, Petzval field curvature, and distortion. The only information found is an exact specification of spherical aberration.

In none of the material found to date is an exact specification for a transmission function of a lens which is appropriate for off-axis radiation (further than the paraxial approximation). The transmission function for the lens is a function of the distance the light travels through the lens, relating that distance to a phase lag the light undergoes. Light incident on a lens surface at an angle larger than zero degrees (off-axis), will travel a further distance than was previously assumed. This additional distance actually yields far larger aberrations than were previously expected for the optical system, thereby significantly degrading system performance.

I.4. Multiple Apertures

A multiple (or synthetic) aperture is formed when separate optical systems are combined to function as a single larger aperture (4:2). Coherent imaging through a synthetic aperture has many advantages, among them ease of manufacturing and reliability (4:2-4). The more apertures contained within a multi-

aperture system the greater the light gathering capability. The central peak of a multi-aperture system is more narrow than that of a single optic which has the same outer, or effective radius. This is advantageous to tracking or two point resolution as was pointed out by Watson (5:40-62).

Coherent imaging through a synthetic aperture, where the dc component of the light has been blocked, also has the added feature of being an edge enhancer. Therefore, there will be "ringing" around any edge of an object coherently imaged through an optical system as shown in Figure 1. Bergey (6:72-75) pointed out that these patterns could be controlled by the number of apertures in the optical system as well as the placement of the apertures in the system.

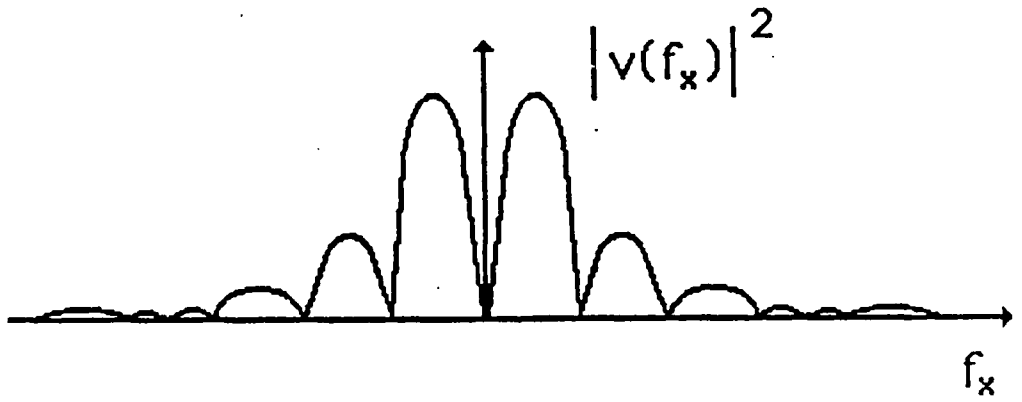

Figure 1. Multiple Aperture Intensity Pattern of an Edge (6:26)

I.5. Aberrations

Aberrations are apparent in any realistic optical system. The third order

aberrations: spherical, astigmatism, coma, distortion, and Petzval field curvature, will be discussed in this thesis. Spherical aberration is dependent upon the fact that the lens is spherical in shape as opposed to aspheric (e.g. hyperbolic). Astigmatism and coma are off-axis effects. If the incident angle of the plane wave with the optic axis is zero, then the effect due to these two aberrations is zero. As the incident angle grows, the effects due to these aberrations grow as well. This greatly affects the final image since the greater the aberration, the greater the beam deformation. Such deformations cause a decrease in field-of-view. Field curvature and distortion only affect the image of an extended object. Since this thesis deals only with the impulse response of the optical systems, these two components of the third order aberrations will be neglected.

When the affects of these aberrations are included in a multi-aperture system, the beam degradation as the incident angle grows will become even more of a problem. The problem with two point resolution in multi-aperture systems is the addition of side lobes, which can be as large if not larger than the central peak (5:40-62). As the incident angle grows, the lobes on one side of the intensity pattern grow much faster than the lobes on the opposite side. This increases the possiblity of error in reading the pattern. Therefore, the beam deformation problem becomes worse in a multi-aperture system. Aberrations are one major limitation to the field-of-view for a multi-aperture optical system.

I.6. Scope

For SDI purposes, optical phased array radars are an optimal solution for tracking and targeting. The requirement of a twenty degree field-of-view means that for far-field imaging a plane wave could be impinging the lens at an angle with respect to the optic axis of twenty degrees or more. The transmittance function for the Goodman thin lens, which has been assumed in all previous work is not applicable for angles in excess of two degrees, as the experimental results showed. Goodman, in defining his thin lens assumed the paraxial approximation. In this thesis, a new definition for the thin lens will be derived which includes the angle of incidence implicitly. The only approximation in this method was to assume that the angle change at the surface due to the index of refraction is negligible.

This thin lens expression was applied to three multi-aperture systems to show how the beam degradation affects the field-of-view as the incident angle is increased. The three multi-aperture systems used are shown in Figure 2. Two of the three multi-aperture systems are being tested at the Air Force Weapons Laboratory, Kirtland Air Force Base, New Mexico. The three aperture system is called Phasar (7) and has been in operation for approximately two years, while the four aperture system is called the Multiple Mirror Tracking Telescope (MMTT) (7), which will begin operation in January 1988. The six aperture system is in the same configuration as the Multiple Mirror Telescope (MMT) in Arizona, where it is engaged in astronomical and other scientific endeavors. Bergey showed that the six aperture system is one of the optimum designs for multi-

aperture systems (6:72-75). Also, Watson (5:40-62) demonstrated that six apertures has a better two point resolution than the other systems he investigated. All of the systems used in this thesis are symmetric with the optical axis as shown and the lenses are separated by a small distance to avoid overlapping in the computational analysis as well as to allow for the fixed supports these systems would require in reality.

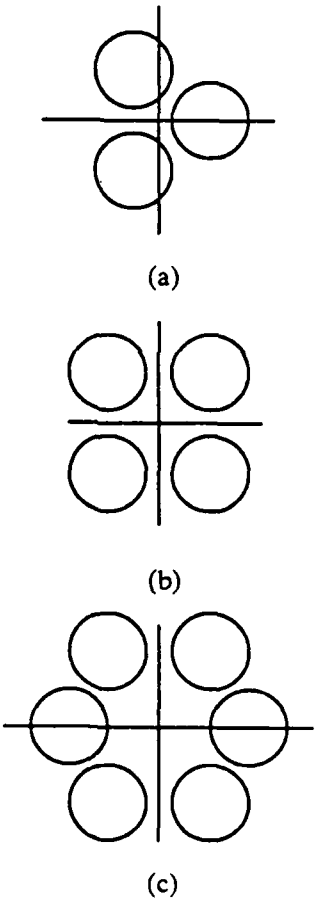

Figure 2. Multi-Aperture Configuration

This thesis will deal strictly with coherent imaging. In Chapter 2, aberrations and Goodman's thin lens will be discussed. The new lens transmittance function will be derived and applied to two different lens designs in Chapter 3. Chapter 4 will verify the methods applied by comparing the previous results with the geometrical ray trace program FALCON and in Chapter 5, experimental analysis is used to support the work done. Chapter 6 will apply thesis lens designs to the three multi-aperture systems. A comparison of these systems will be made in Chapter 7 and the conclusions drawn will be presented in Chapter 8.

II. Aberrations and the Perfect Thin Lens

This chapter develops the concept of aberrations and the perfect thin lens. Aberrations, as discussed by Born and Wolf (8:459-490), will be applied to an optical model. The aberration coefficients are then derived for practical comparisons of these optical models, and the case of Goodman's thin lens applied. This model was computationally analyzed and the resulting intensity patterns are given at the end of this chapter. In addition, the lens parameters of the thin and thick lenses used in all of the analyses in this thesis are included.

II.1. Aberrations

The following development follows closely that of Born and Wolf (8:460-472). Consider the centered optical system shown in Figure 3:

In order to get a perfect Airy pattern (8:460) in the image plane, a perfect but truncated spherical wave must exit the lens system (at the exit pupil). However, if a wavefront exits the lens system and is different from a perfect spherical wave, then aberrations exist which are of the form Q - $\bar{Q}$, (the distance between the two wavefronts). It is convenient to regard ϕ as the total effect due to aberrations, where ϕ is of the form:

$$\phi = \phi(Y_1^*, \rho, \theta) \tag{2.1}$$

and:

Y_1^* = *object height from the optic axis in the image plane*

ρ = *radial distance from the optic axis in the plane of the exit pupil*

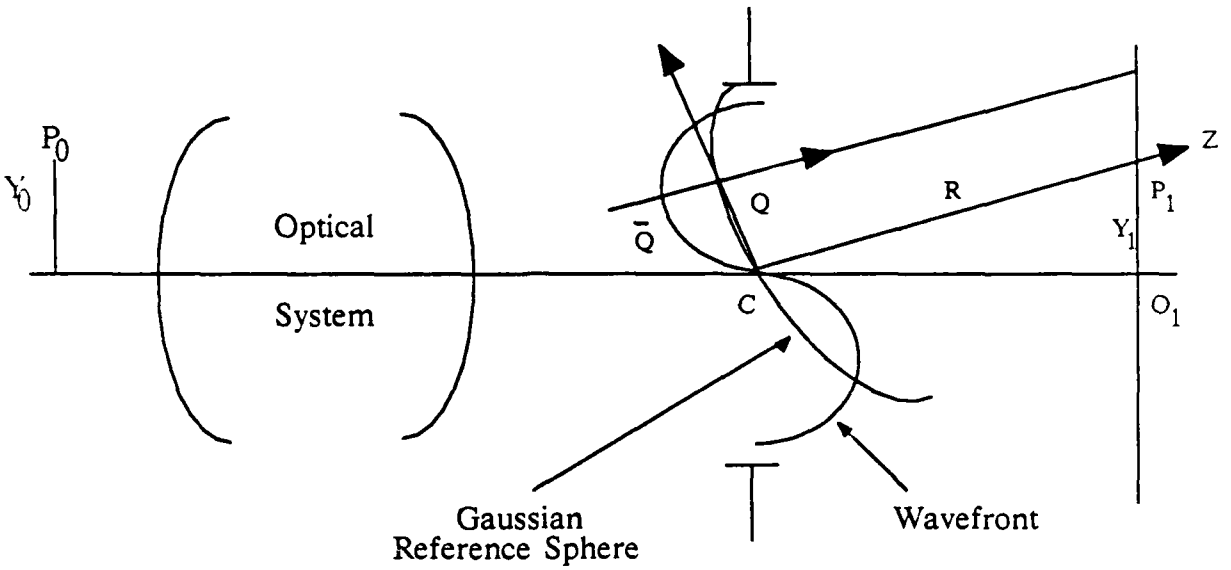

Figure 3. Reference Frame and Notation for Aberration Analysis

θ = angle of rotation around the optic axis in the plane of the exit pupil

Including aberrations, the Huygens-Fresnel equation becomes:

$$U(x_1,y_1) = \left(\frac{-j}{\lambda z}\right)\exp(-jkz)\int\int\left(\frac{\exp jk(\phi+s)}{s}\right)dS \qquad (2.2)$$

Where dS is the spatial integration over the exit pupil, lambda is the wavelength of interest, k is the wave number, and z and s are optical path differences from the object to image planes.

The function ϕ can be separated in many fashions. Two of the most famous ways are given by Seidel and Zernike. The Seidel aberrations are defined for geometrical optics, whereas, the Zernike circle polynomials were defined for

diffraction analysis. The representations for the primary aberrations in both forms is given below in Table II-1, where the expansions for ϕ are given by:

$$Seidel: \ \phi = A'_{lnm}\rho^n \cos^m\theta \tag{2.3}$$

$$Zernike: \ \phi = \epsilon_{nm} A_{lnm} R_n^m(\rho)\cos m\theta \tag{2.4}$$

TABLE II-1.

Representation of the Primary Aberrations

Aberration	l	n	m	Seidel Form	Zernike Form
Spherical	0	4	0	$A'_{040}\rho^4$	$\frac{1}{\sqrt{2}}A_{040}R_4^0(\rho) = \frac{1}{\sqrt{2}}A_{040}(6\rho^4 - 6\rho^2 + 1)$
Coma	0	3	1	$A'_{031}\rho^3\cos\theta$	$A_{031}R_3^1(\rho)\cos\theta = A_{031}(3\rho^2 - 2\rho)\cos\theta$
Astigmatism	0	2	2	$A'_{022}\rho^2\cos^2\theta$	$A_{022}R_2^2(\rho)\cos 2\theta = A_{022}\rho^2(2\cos^2\theta - 1)$
Field Curvature	1	2	0	$A'_{120}\rho^2$	$\frac{1}{\sqrt{2}}A_{120}R_2^0(\rho) = \frac{1}{\sqrt{2}}A_{120}(2\rho^2 - 1)$
Distortion	1	1	1	$A'_{111}\rho\cos\theta$	$A_{111}R_1^1(\rho)\cos\theta = A_{111}\rho\cos\theta$

From Eq. (2.2), the transfer function G can be defined as follows:

$$G(x_0, y_0) = \exp(ik\phi) \tag{2.5}$$

where G contains all of the contributions to the image due to aberrations. Therefore, all of the aberration effects produced by an optical system can be combined into one function which is applied at the exit pupil of the system. Thus, it can be

said that the optical system is perfect, but there is a transparency across the exit pupil , G, which contains all of the aberrations. The sole effect of these aberrations is seen to be the introduction of phase distortions within the bandpass of the system. These phase distortions can have a severe effect on the fidelity of the system (1:121).

II.2. Lens Design

Two lenses were used in the experimental analysis. These lenses were then used to test out the analytical and computational portions of this thesis. The first lens was a thin lens which was chosen to verify the computational analyses, while the second lens was chosen as a thick lens to show the limitations of the analyses. Given:

LENS 1:

$$R_1 = 16.84cm$$

$$R_2 = -44.23cm$$

$$H = 4.372cm$$

$$On-axis\ thickness = .794cm$$

and

$$n = 1.5$$

Where n is the index of refraction for any non-specific glass. The second lens was designed to test the limits of the approximations made. Lens 2 is a thick lens which will have large aberrations present:

LENS 2:

$$R_1 = 11.37cm$$

$$R_2 = -11.63cm$$

$$H = 6.0976cm$$

$$On-axis\ thickness = 3.5cm$$

and

$$n = 1.5$$

The aperture stop in both optical systems is 1 cm in radius.

II.3. Perfect Thin Lens

A lens is said to be a thin lens if a ray entering at coordinates (x,y) on one face emerges at approximately the same coordinates on the opposite face, i.e., if there is negligible translation of the ray within the lens (1:77). Figure 4 gives the description of the lens used in this discussion. This discussion follows Goodman (1:77-85).

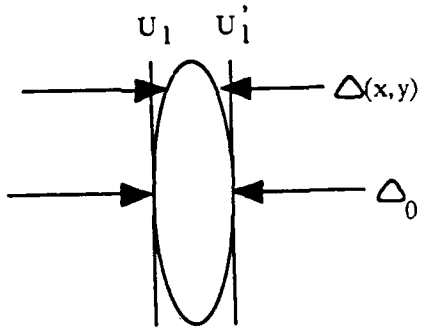

Figure 4. Goodman's Thin Lens

The phase delay given to an incident wave going through this lens is:

$$\phi(x,y) = kn\nabla(x,y) + k(\nabla_0 - \nabla(x,y)) \qquad (2.6)$$

Where n is the index of refraction, the first term is the phase delay introduced by the lens and the second term is the phase delay introduced by the remaining region of free space between the two planes. Therefore, the transmittance function of the thin lens is given by:

$$t_l(x,y) = \exp(jk\nabla_0)\exp(jk(n-1)\nabla(x,y)) \tag{2.7}$$

And, the complex field immediately behind the lens is:

$$U_l'(x,y) = t_l(x,y)U_l(x,y) \tag{2.8}$$

Thus, the problem is to define the thickness function of the lens, $\nabla(x,y)$. To define this, break up the lens into two separate parts, as shown in Figure 5. Then the problem is to solve for each half of the distance, or phase delay, that the lens imparts.

After solving for distances the light travels in the lens, ∇_1 and ∇_2 are given by:

$$\nabla_1(x,y) = \nabla_{01}-(R_1-[R_1^2-x^2-y^2]^{\frac{1}{2}}) \tag{2.9}$$

$$\nabla_2(x,y) = \nabla_{02}-(-R_2-[R_2^2-x^2-y^2]^{\frac{1}{2}}) \tag{2.10}$$

Adding the terms together, remembering that $\nabla_{01}+\nabla_{02}=\nabla_0$:

$$\nabla(x,y) = \nabla_0-R_1\left(1-\left[1-\frac{(x^2+y^2)}{R_1^2}\right]^{\frac{1}{2}}\right)+R_2\left(1-\left[1-\frac{(x^2+y^2)}{R_2^2}\right]^{\frac{1}{2}}\right) \tag{2.11}$$

The most important approximation taken in Goodman's analysis is the paraxial approximation. After completing the binomial expansion of the two square roots, this approximation requires that only the first two terms are retained and all other terms are ignored. This assumes that the radii of the two spheres which make up the thin lens are much greater than the radius of the lens itself (or the distance from the optic axis). After this assumption is made, the

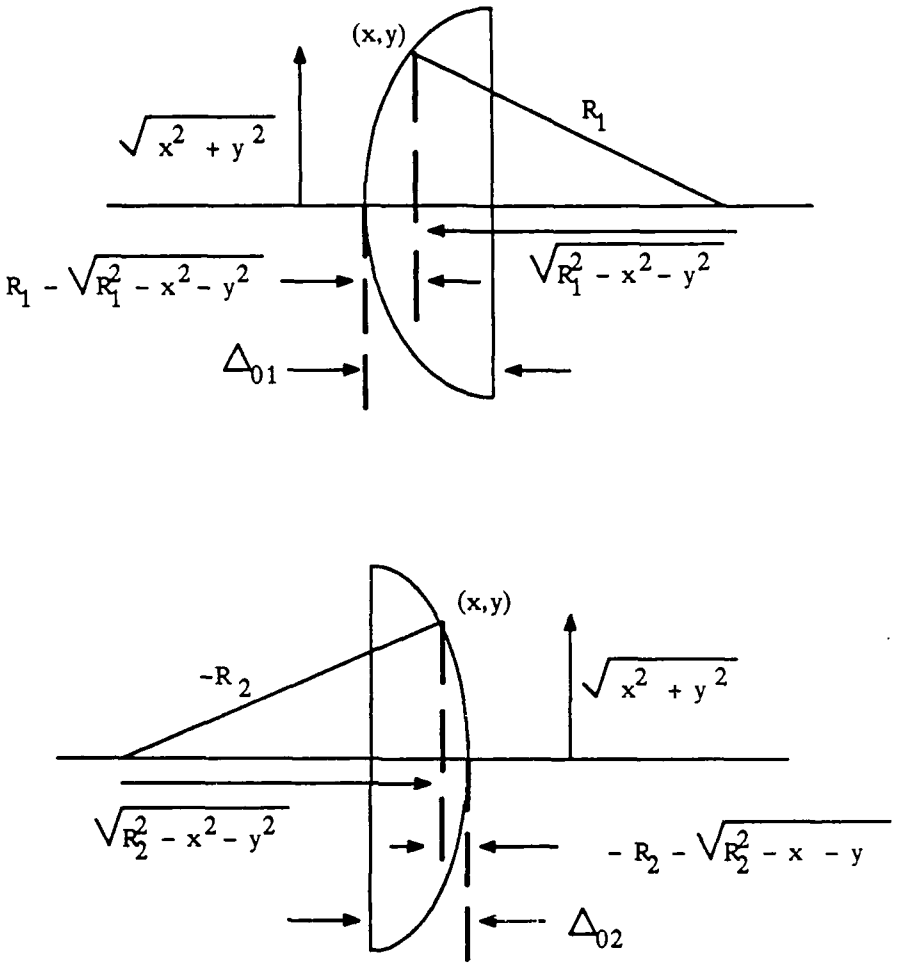

Figure 5. Calculation of the Thickness Function

new equation for ∇ is:

$$\nabla(x,y) = \nabla_0 - \frac{(x^2+y^2)}{2}\left(\frac{1}{R_1} - \frac{1}{R_2}\right) \tag{2.12}$$

Substituting this expression into Eq. (2.7) and remembering the len's makers equation:

$$\frac{1}{f} = (n-1)\left(\frac{1}{R_1} - \frac{1}{R_2}\right) \tag{2.13}$$

The final equation for the perfect thin lens is then:

$$t_l(x,y) = \exp\left[\frac{-jk}{2f}(x^2+y^2)\right] \tag{2.14}$$

Where the exponential phase factor $exp(jkn\nabla_0)$ can be ignored since we are only looking at the intensity patterns in this thesis. When this equation is used to find the complex field amplitude, (ignoring the phase factors in front of the integral since they will negate when computing the intensity) the new complex amplitude is found via the Fresnel transform :

$$U(x_0,y_0) = \int\int U(x_1,y_1)\exp\left[\frac{jk}{2f}(x^2+y^2)\right]\exp\left[-\frac{j2\pi}{\lambda f}(x_0x_1+y_0y_1)\right]dx_1dy_1 \tag{2.15}$$

Here $U(x_1,y_1)$ is now only a function of the shape of the exit pupil, in this case a lens (a circle). The limits of the integral then become the limits of the aperture. Given in Figure 6 is the intensity pattern of a circular aperture containing a perfect thin lens in a plane a focal length away. This pattern is called the Airy pattern, named after G. B. Airy (9).

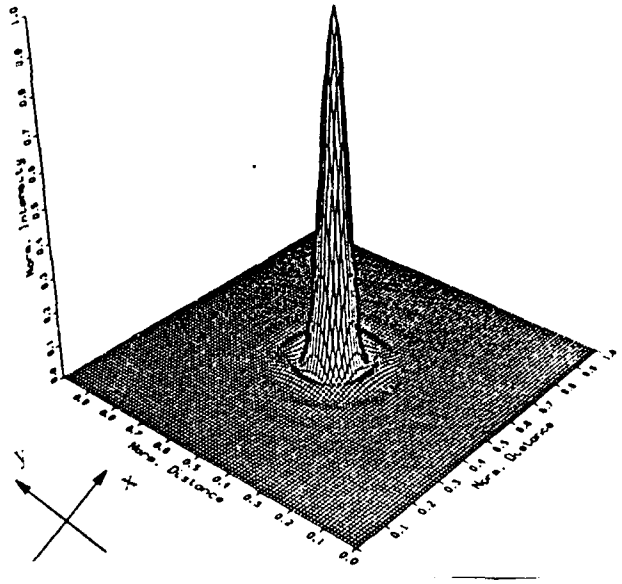

Figure 6. The Airy Pattern

However, in taking the paraxial approximation, Goodman excluded any effects of aberrations as can be shown in Geary's paper (3:52-54). In excluding all of these aberrations, there would be no beam deformation as the angle of incidence grows. In the following analysis, the binomial approximation will not be taken. Therefore, the transfer function for Goodman's thin lens becomes:

$$t_i(x,y) = \exp\left[jk(n-1)\left[-R_1\left(1-\left[1-\frac{(x^2+y^2)}{R_1^2}\right]^{\frac{1}{2}}\right)+R_2\left(1-\left[1-\frac{(x^2+y^2)}{R_2^2}\right]^{\frac{1}{2}}\right)\right]\right] \quad (2.16)$$

When this equation is used to find the field amplitude using the Fresnel transform, the intensity pattern is derived and given below in Figure 7.

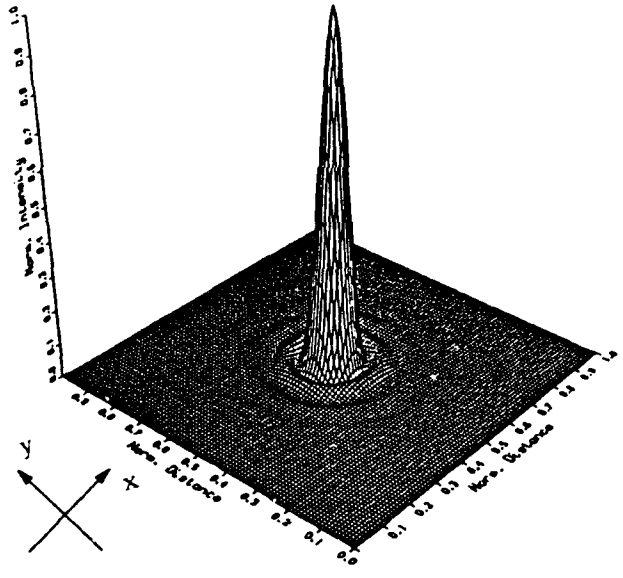

Figure 7. Goodman Analysis at $\alpha = 0$

Note that the main aberration affecting the system is spherical aberration. The second ring of the pattern is .0190 times the height of the central maximum whereas in an unaberrated case the second ring would be .0175 times the central

maximum. As long as the plane wave is parallel to the optic axis, the contributions due to astigmatism and coma are zero.

Goodman handles an off-axis plane wave as a function of the input U(x,y). Figure 8 below shows the system used.

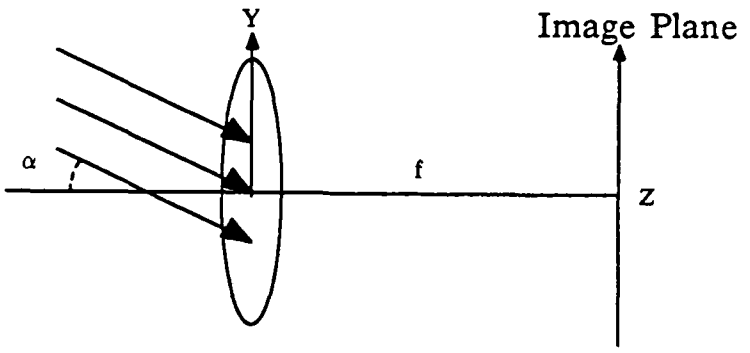

Figure 8. The General Thin Lens Configuration

The input plane wave then becomes:

$$U_l(x,y) = \exp(jk\sin\alpha\, y) \tag{2.17}$$

versus one for a unit amplitude plane wave parallel to the optic axis, and alpha is the angle in the y-z plane with respect to the z or optic axis. The complex amplitude can still be solved with the methodology given previously. The complex amplitude in the image plane was solved by taking the Fast Fourier Transform (FFT) of the plane wave incident on a thin lens. The output of the FFT was then squared to obtain the intensity distribution in the image plane. The program used for this analysis is located in Appendix A. The intensity patterns for various angles alpha are shown in Figure 9 for Lens 1 and in Figure 10 for Lens 2. The Strehl Ratios for the intensity patterns decrease as the angle alpha increases. Here, the Goodman case analyzed still carries all of the contributions due to

spherical aberration and defocus, and as can be seen in Chapter 4, as the angle is increased, the Zernike coefficient for spherical aberration increases a finite amount due to the changing defocus term. Therefore the Strehl Ratio should correspondingly decrease by a finite amount as is shown in the two figures.

As is shown in the previous graphs, the plane wave at an arbitrary angle alpha just moves the $\alpha = 0$ pattern up and down the image plane with respect to the magnitude of alpha, i.e., the larger the angle alpha, the larger the displacment in the image plane from the optic axis. Therefore in the Goodman case, the angle alpha does not affect the amount of aberrations at all, the aberrations are all contained in the transfer function within the square root. From this result there whould be no beam degradation at all as the field-of-view is increased. However, this is known not to be true, based on experimental evidence obtained using PHASAR at the Air Force Weapons Laboratory (7). Therefore, this description of a thin lens must be incorrect.

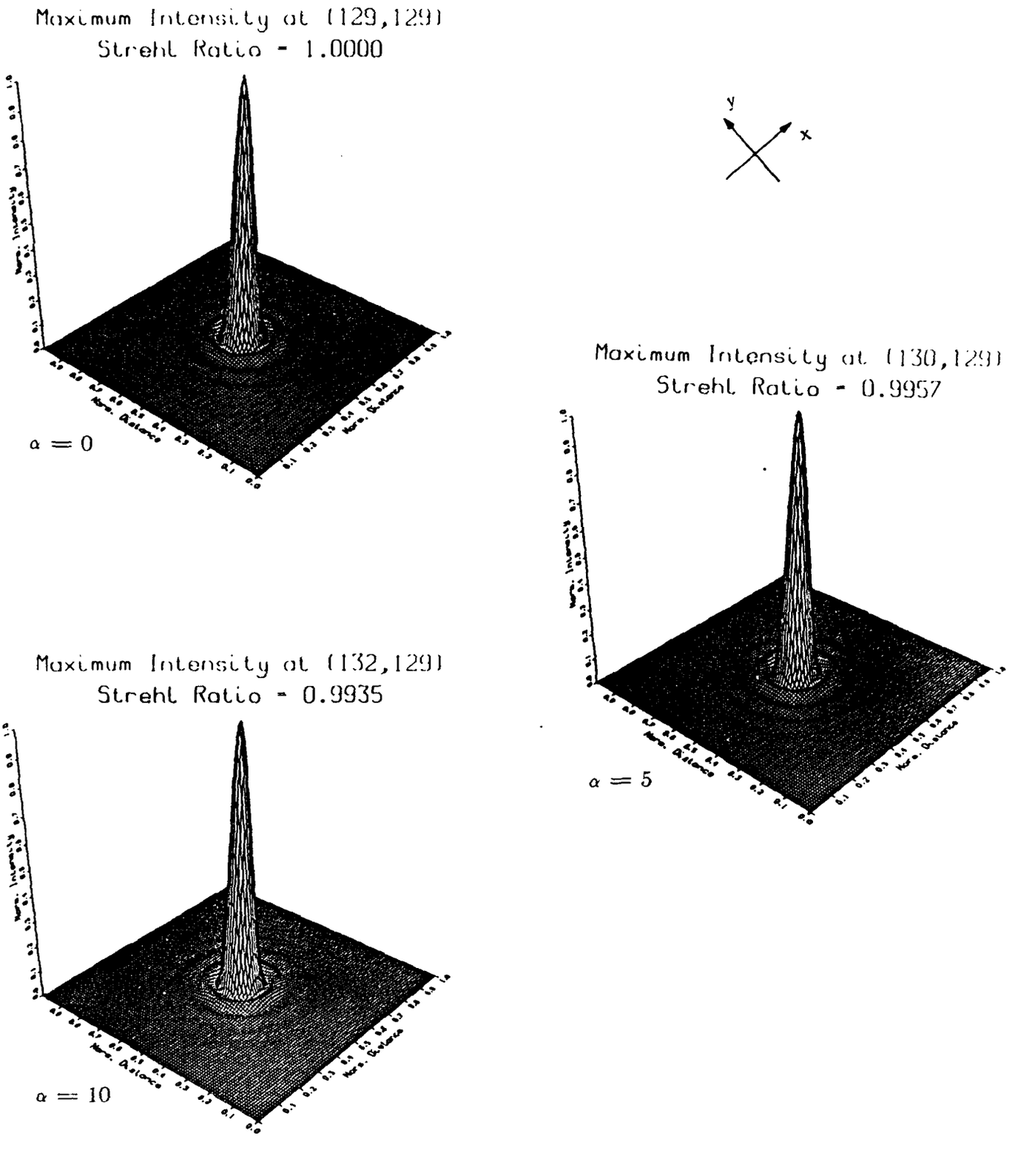

Figure 9. Goodman Analysis, Lens 1, for $\alpha = 0$, 5, and 10 Degrees

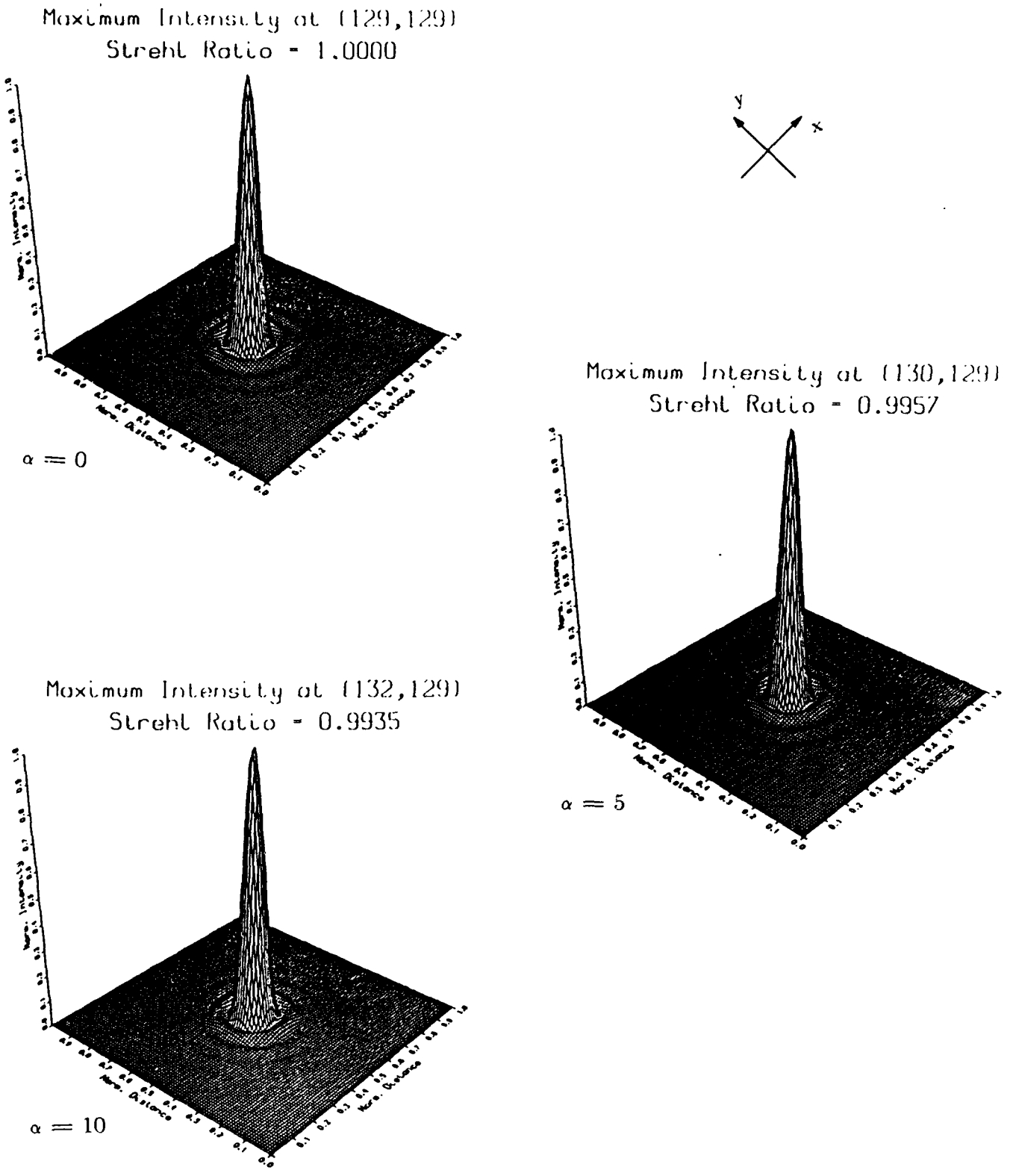

Figure 10. Goodman Analysis, Lens 2, for $\alpha = 0$, 5, and 10 Degrees

III. A New Thin Lens Expression (The Walton Thin Lens)

This chapter explores the expression of a thin lens which is applicable for off-axis projections such as those used in multi-aperture systems. An expression is derived and then computationally analyzed. Following this are several verifications of the expression's accuracy. The Strehl ratios for all of the cases are presented as well as the limiting case at $\alpha = 0$ which should approach an Airy pattern. Also included are the cross-sections at various angles to determine which aberrations are present and which aberrations cause most of the beam deformation as the angle alpha grows.

III.1. The Mathematical Expression

Figure 11 describes the system employed in the following analysis. The center of the coordinate system is at the "center" of the lens, or where the two halves of the lens meet at the optic axis. The only approximation made in this case is that the lens is a thin lens, i.e., that one can ignore the refraction of light at the lens surface. To make the mathematics managable, alpha, the angle of the incident plane wave with the optic axis, is taken to be with respect to the y-z plane only. The thin lens approximation also states that throughout the system, the plane wave will stay in a specific y-z plane for any given value of x.

The next part of the analysis is purely geometrical, with many of the details omitted. First, the lens thickness is solved for as in Chapter 2. This new thickness is substituted in for ∇ in Eq. (2.12) giving the transmittance function for the

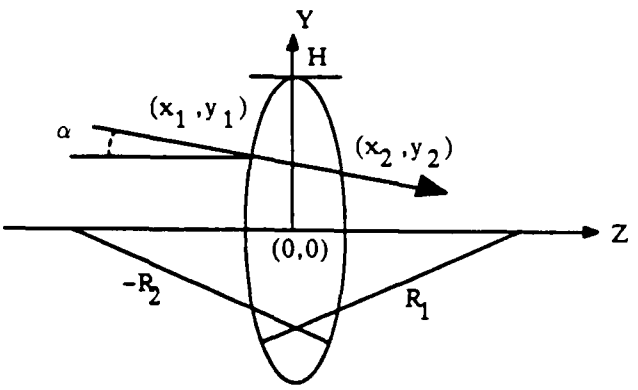

Figure 11. Geometry Used for Walton Thin Lens

new lens expression.

To solve for the distance between the two surfaces of the lens, the equations of the two spheres and the equation for the line, which is two-dimensional since the plane wave is only in the y-z plane, are equated. To solve for the point at which the entering ray exits the lens, equate, for the:

$$Sphere : (\nabla + z_2)^2 + x_2^2 + y_2^2 = R_2^2 \tag{3.1}$$

$$Line : y_2 = -\tan\alpha(z_2 - z_0) + y \tag{3.2}$$

Where the point $(y, z_0) = (y,0)$, so that or the reference frame of the lens becomes the x-y plane. Also:

$$\nabla = \left(R_2^2 - H^2\right)^{\frac{1}{2}} \tag{3.3}$$

Solving these two equations yields a quadratic equation in z_2:

$$z_2^2(sec^2\alpha) + 2z_2\left(\left(R_2^2 - H^2\right)^{\frac{1}{2}} - y\tan\alpha\right) + x_2^2 + y^2 - H^2 = 0 \tag{3.4}$$

or

$$\beta z_2^2 + 2\zeta_- z_2 + \eta = 0 \tag{3.5}$$

where

$$\beta = \sec^2\alpha$$

$$\varsigma_- = \left(R_2^2 - H^2\right)^{\frac{1}{2}} - y\tan\alpha \tag{3.6}$$

$$\eta = x_2^2 + y^2 - H^2$$

Solving for the point (y_2, z_2) :

$$z_2 = -\left(\frac{\varsigma^-}{\beta}\right) + \left(\left(\frac{\varsigma^-}{\beta}\right)^2 - \frac{\eta}{\beta}\right)^{\frac{1}{2}} \tag{3.7}$$

$$y_2 = -z_2\tan\alpha + y$$

In a similar manner, the following three equations are solved for the point (y_1, z_1):

$$Sphere : (z_1 - \nabla')^2 + x_1^2 + y_1^2 = R_1^2 \tag{3.8}$$

$$Line : y_1 = -\tan\alpha(z_1 - z_0) + y \tag{3.9}$$

$$\nabla' = \left(R_1^2 - H^2\right)^{\frac{1}{2}} \tag{3.10}$$

Where again, the reference of the x-y axis through the origin was used such that the point $(y, z_0) = (y,0)$. Solving these three equations as before gives the point (y_1, z_1) with respect to y and alpha:

$$z_1 = \left(\frac{\varsigma_+}{\beta}\right) - \left(\left(\frac{\varsigma_+}{\beta}\right)^2 - \frac{\eta}{\beta}\right)^{\frac{1}{2}} \tag{3.11}$$

$$y_1 = -z_1\tan\alpha + y \tag{3.12}$$

where:

$$\beta = \sec^2\alpha$$

$$\varsigma_+ = \left(R_1^2 - H^2\right)^{\frac{1}{2}} + y\tan\alpha \tag{3.13}$$

$$\eta = x_1^2 + y^2 - H^2$$

Therefore, to solve for the distance between the two surfaces as a function of the system parameters (R_1, R_2, and H) and the givens (x, y, and α) the distance formula is needed. The distance is then given by:

$$d(P_2,P_1) = \left((z_2-z_1)^2+(y_2-y_1)^2\right)^{\frac{1}{2}} \tag{3.14}$$

This form is two-dimensional in y and z because of the thin lens approximation. Substituting in for the two points derived above, the distance formula becomes:

$$d = \cos\alpha\left(\left(\varsigma_-^2-\eta\beta\right)^{\frac{1}{2}}+\left(\varsigma_+^2-\eta\beta\right)^{\frac{1}{2}}-\varsigma_--\varsigma_+\right) \tag{3.15}$$

where

$$\begin{aligned}
\beta &= \sec^2\alpha \\
\varsigma_- &= \left(R_2^2-H^2\right)^{\frac{1}{2}}-y\tan\alpha \\
\varsigma_+ &= \left(R_1^2-H^2\right)^{\frac{1}{2}}+y\tan\alpha \\
\eta &= x^2+y^2-H^2
\end{aligned} \tag{3.16}$$

Therefore the new transfer function for the thin lens becomes:

$$t_l(x,y) = \exp(jk(n-1)d) \tag{3.17}$$

The constant phase factor was again ignored since only intensity patterns are being considered.

III.2. Computational Analysis

The intensity patterns were solved by taking the FFT of a plane wave incident on a thin lens. The output of the FFT was then squared to obtain the intensity distribution in the image plane. The program ALPHA written for this purpose is included in Appendix B. The thin lens was described as a set of distances from which a set of optical path differences was defined. In Figure 12 are two graphs which depict the distances the light travels through the lens. Part (a) shows the set of distances for an angle of $\alpha = 0$; part (b) the set of distances for

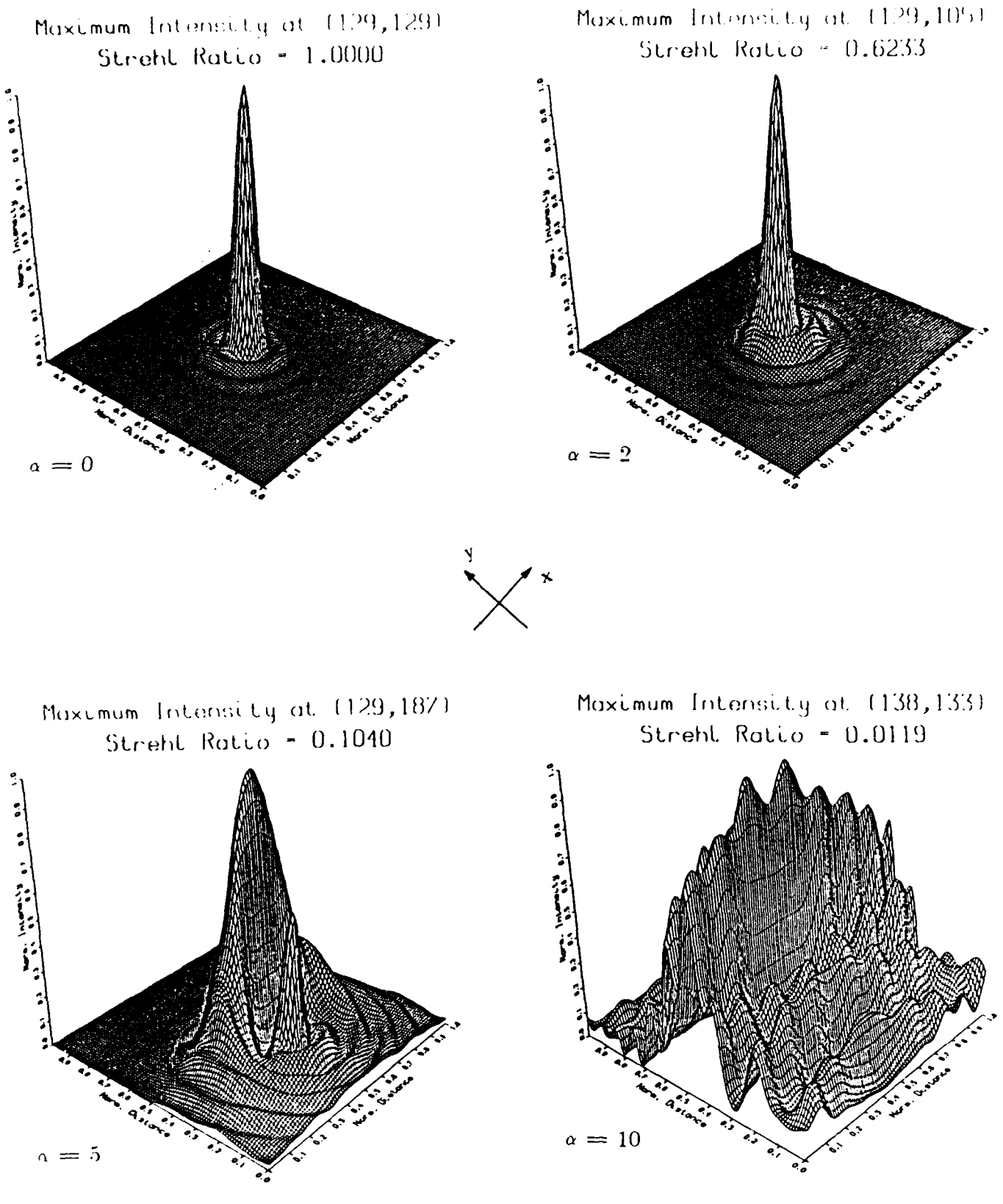

Figure 13. Walton Analysis, Lens 1, for $\alpha = 0, 2, 5$, and 10 Degrees

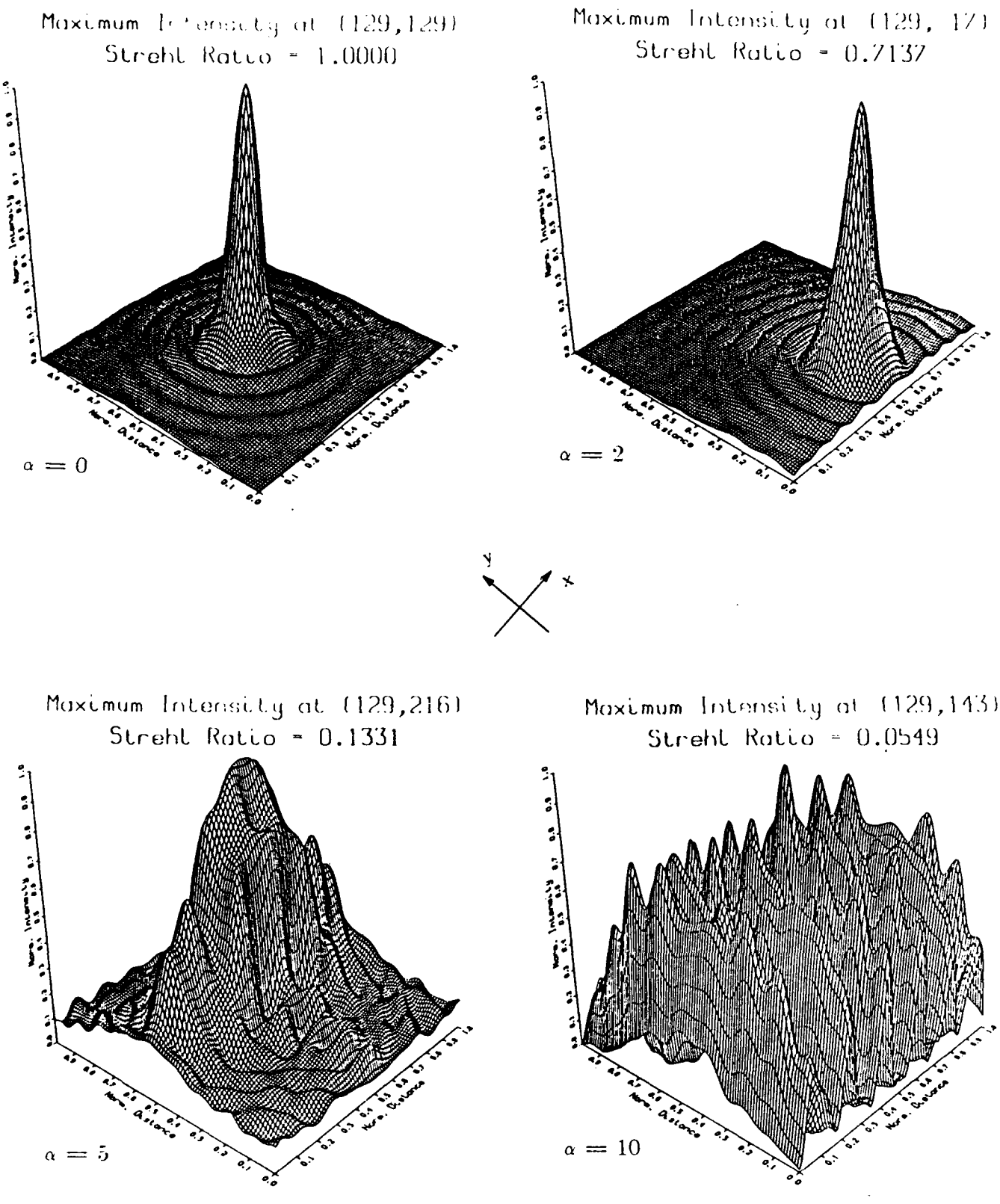

Figure 14. Walton Analysis, Lens 2, for $\alpha = 0, 2, 5,$ and 10 Degrees

Next, the Strehl Ratios were calculated for all of the intensity patterns. As can be seen, for the thin lens the Strehl ratios correlate well with information given by Mills (10). A significant problem deduced from the Strehl Ratios is that the power in the central peak has decreased by 40 percent as the angle alpha has increased to two degrees in Lens 1. Lens 2 shows that there is a valid problem with the approximation made when the lens varies at all from being "thin". This correlates well since Lens 2 was designed to be a thick lens. The distance formula derived above is therefore inappropriate for a lens of this type.

The last verification made was to vary the size of the aperture stop to show how the aberrations change. The smaller the aperture stop, the more like an Airy pattern the diffraction pattern becomes. The larger the aperture stop, the more aberrations there are present in the diffraction pattern. This is shown in Figure 15.

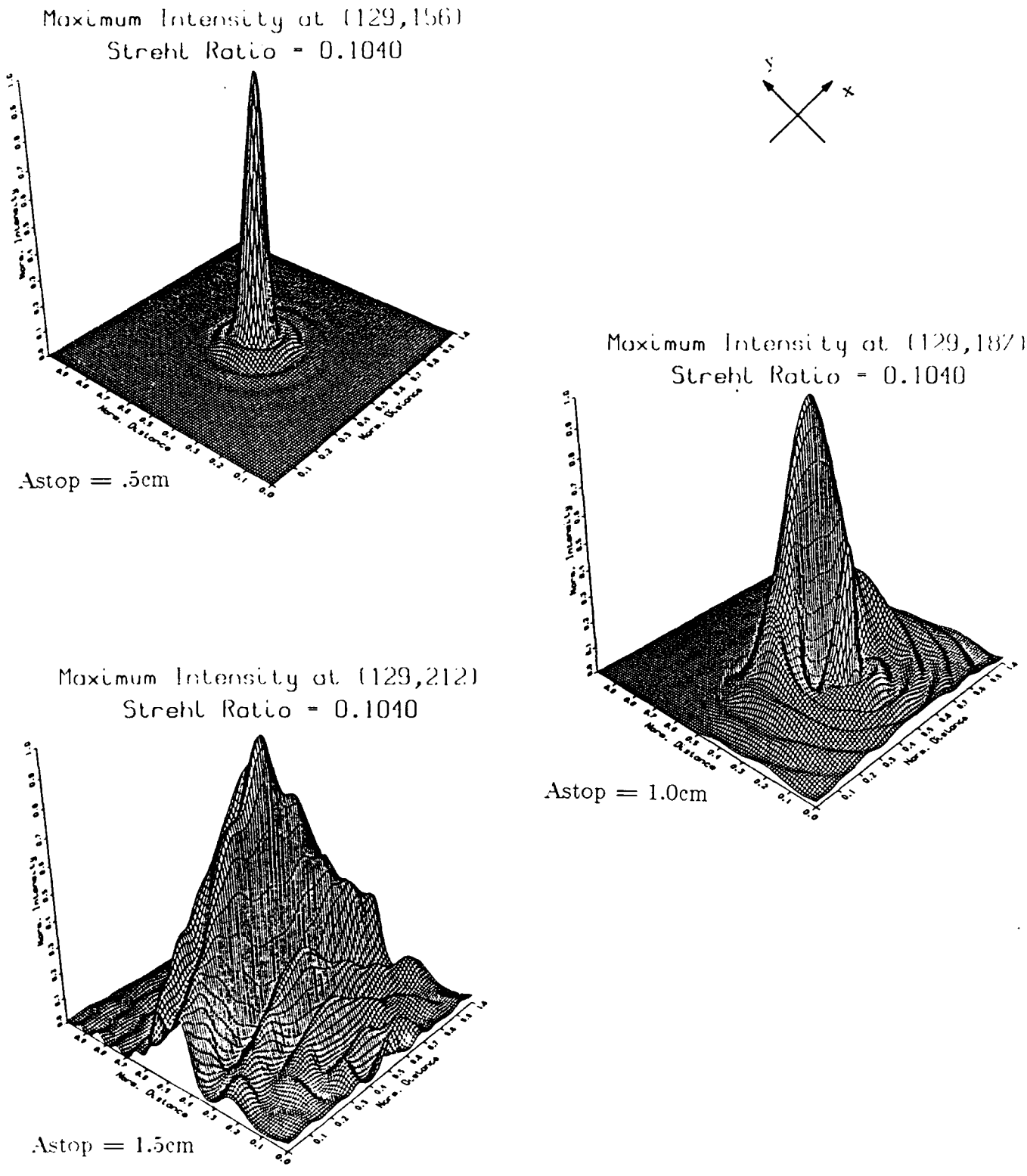

Figure 15. Aperture Stop = .5, 1.0, 1.5 cm for Lens 1 at $\alpha = 5$ Degrees

IV. Analysis Using FALCON, a Geometrical Ray Trace Program

In the previous chapter, the Walton Thin Lens expression was analyzed for on-axis cases. In this chapter, the expression is compared to the geometrical solution for off-axis projections. The geometrical ray trace program FALCON was used to derive the aberration coefficients which were used in a diffraction analysis and subsequently compared to the Walton expression. The program written to compute the diffraction analysis is included in Appendix C. The intensity plots derived for this analysis are given at the end of the chapter.

IV.1. FALCON

A comparison was made between the Walton Thin Lens and the results from the geometrical ray trace program FALCON (11). Initially the lens characteristics were first entered into FALCON, and since a geometrical analysis requires an object, an object of variable height was place at "infinity" so that a plane wave of various angles could be modelled. The results, the aberration coefficients, were then computed and inserted into a diffraction analysis. The aberration coefficients for piston, tilt, and defocus were included in the diffraction analysis for complete accuracy, but are not included below because the emphasis in this thesis is the beam deformation due to the third order aberrations. Listed below are the approximate coefficients for the two lenses used in this analysis. As can be seen from the intensity patterns in Figures 16 and 17, the aberrations occured at a much smaller angle than they did in the Walton analysis. However, the two ana-

lyses definitely show similarities in the shape of the resultant curves and in the aberrations which dominate as the angle alpha grows. Table III-1 lists the various aberration coefficients for the two lenses at various angles alpha.

As can be seen from the intensity plots for the diffraction analysis, the plots for the thin lens correlate with those from the Walton analysis. Because of this correlation, these coefficients are a close approximation to the actual coefficients. However, the thick lens did not correlate as well in this case, so the coefficients for the second lens are not a good approximation. This is due to the program being inadequate in the limit of the thick lens. Therefore, the intensity plots for the thick lens will not be representative of the actual intensity distributions.

From the analysis of FALCON, the diffraction analysis seems to break down as the angle alpha grows above ten degrees for the thin lens, and five degrees for the thick lens. This is delineated in the next chapter as the aberration coefficients grow out of proportion to the experimental analyses.

Table III-1 Aberration Coefficients for Lens 1 and Lens 2

LENS 1

Angle	45 Astig.	90 Astig.	X Coma	Y Coma	Spherical
0	0.0	0.0	0.0	0.0	-0.0424
2	0.1744	0.0	0.0	0	0.0735
5	1.1094	0.0	0.0	0.1931	-0.0444
10	4.7075	0.0	0.0	0.4541	-0.0506
15	11.6450	0.0	0.0	0.8712	-0.0630
20	23.5473	0.0	0.0	1.5881	-0.0873

LENS 2

Angle	45 Astig.	90 Astig.	X Coma	Y Coma	Spherical
0	0.0	0.0	0.0	0.0	-0.5387
2	.3198	0.0	0.0	0.6530	-0.5478
5	2.0326	0.0	0.0	1.6826	-0.5715
10	8.6280	0.0	0.0	3.7407	-0.6643
15	21.2976	0.0	0.0	6.6225	-0.8462
20	42.8664	0.0	0.0	11.0306	-1.1836

All of these coefficients have the units of waves or optical path difference.

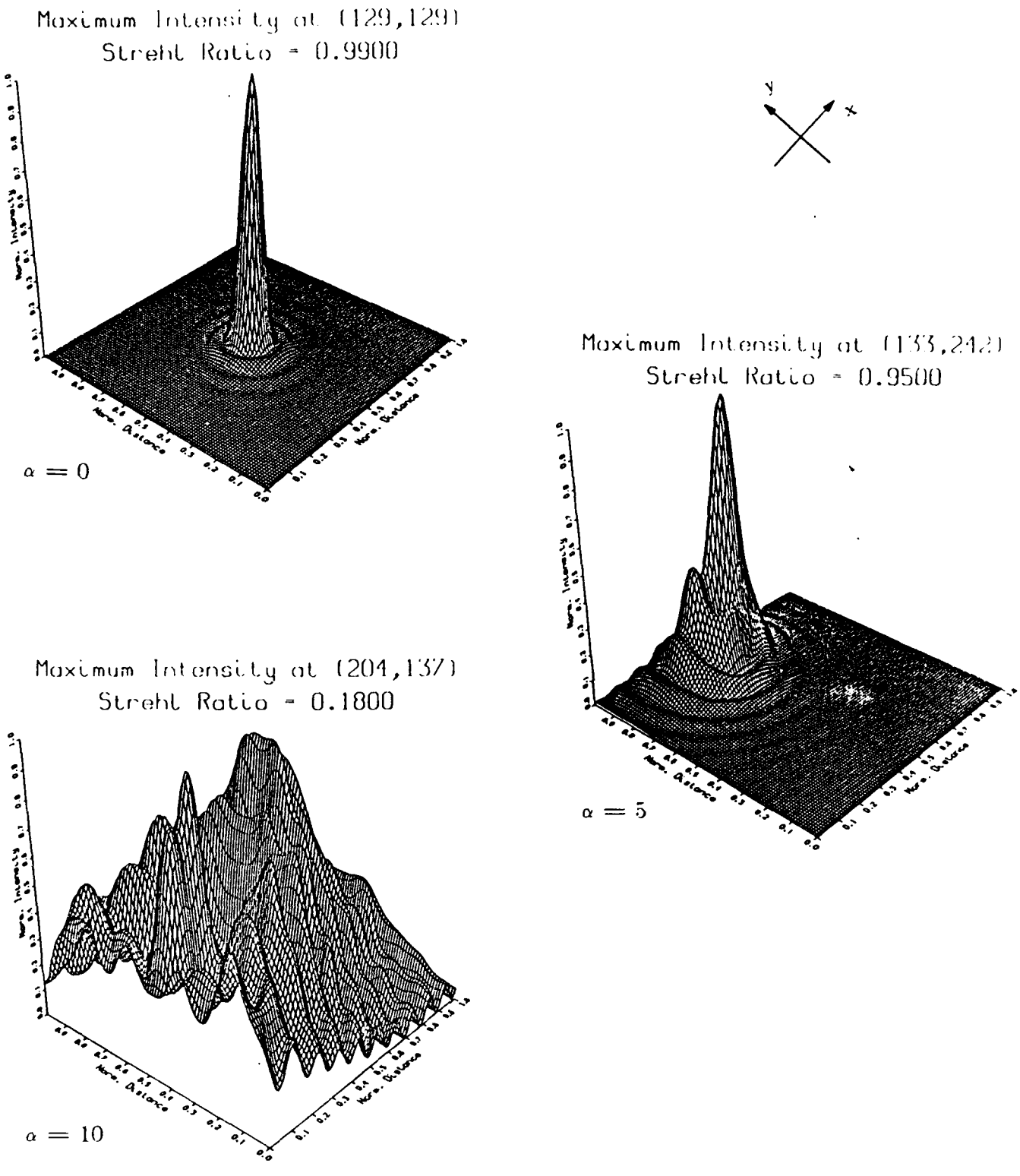

Figure 16. FALCON Analysis, Lens 1, for $\alpha = 0$, 5, and 10 Degrees

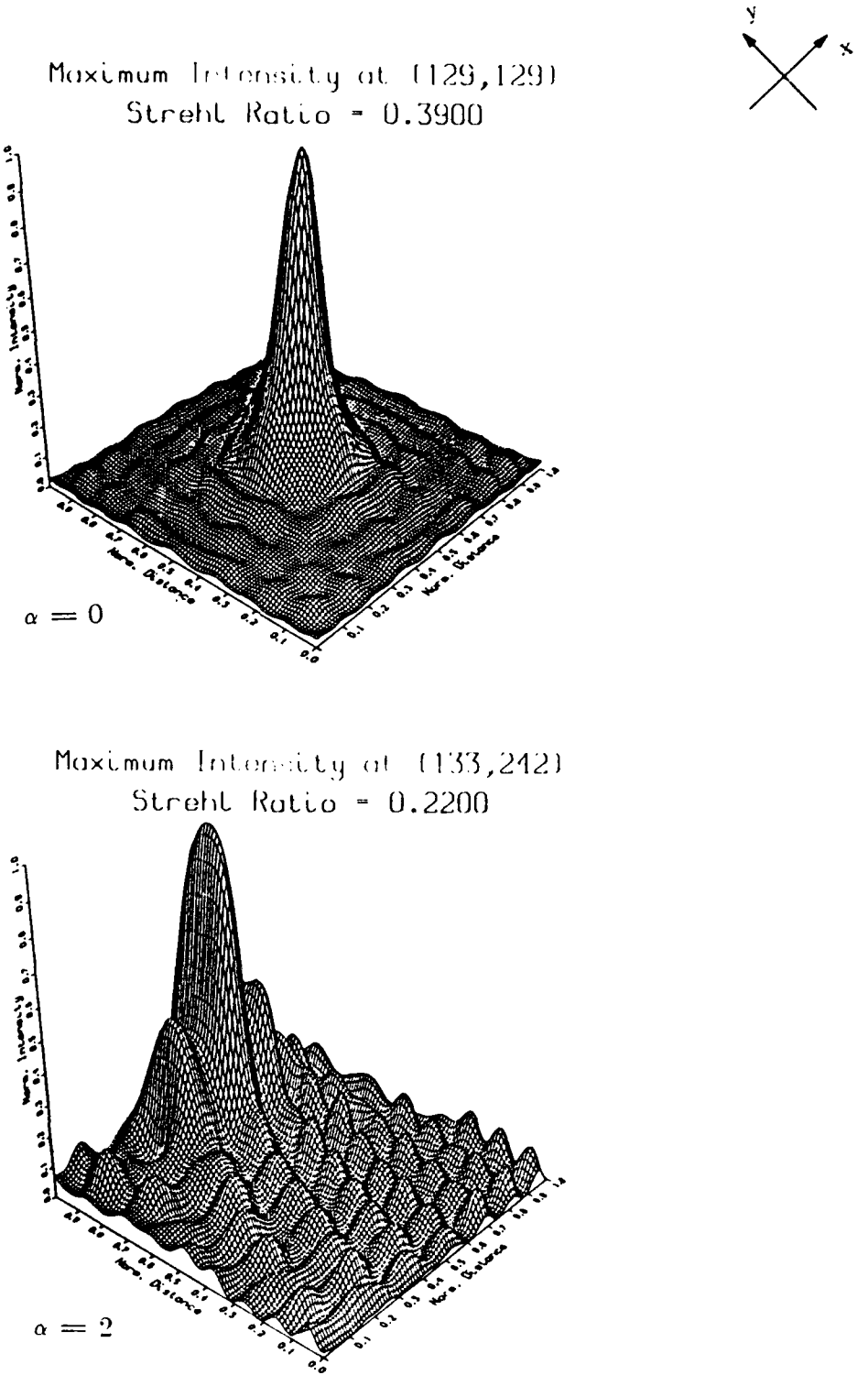

Figure 17. FALCON Analysis, Lens 2, for $\alpha = 0$ and 2 Degrees

V. Experimental Verification

The most important verification for this new expression is a comparison to experimental results. Below is the experimental set-up which was used to verify the impulse response of a lens. The lens was turned through different angles to simulate radiation which would impinge the static lens from various angles in reality. The experimental results versus the computational results are outlined below.

V.1. The Experiment

Figure 18 gives the experimental set-up used to validate the previous analysis.

The two lenses described in Chapter 2 were used in this set-up. As a reminder, the first lens was a thin lens with dimensions of $R_1 = 16.84$ cm, $R_2 = 44.23$ cm, H = 4.37 cm, and an aperture stop with a radius of 1 cm. The second lens had dimensions of $R_1 = 11.37$ cm, $R_2 = -11.63$ cm, H = 6.09 cm, and an aperture stop with a radius of 1 cm. A HeNe laser was used in the experiment and in all of the previous analyses as well. True to assumptions, the thicker the lens, the worse the aberrations became as the angle of incidence of the radiation grew.

V.2. Results

The results of the experiment are shown in Figures 19 and 20. These intensity patterns are not normalized to any size standard, as the analysis is purely

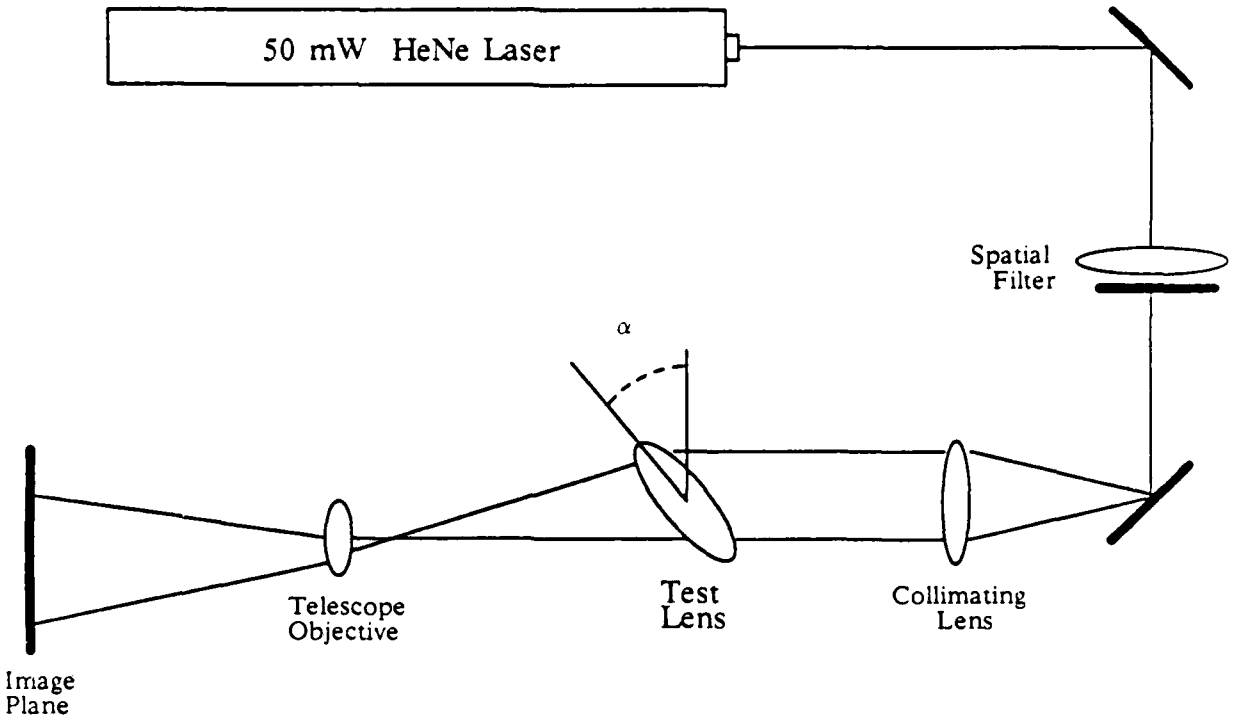

Figure 18. Experimental Set-Up

qualitative not quantitative. The larger the off-axis angle, the larger the pattern in the far-field. The distance to the image plane is given for each set of pictures. A correct size approximation can be made based on the distance from the telescope to the camera, which was chosen in order to get the most information per picture. All pictures were taken with the same shutter speed and f number, however, various neutral density filters were required. The magnitudes of these filters are also given in the above figures. These magnitudes are representative of the magnitudes of the intensity in the central peak. The larger the neutral density filter, the larger the intensity value. As can can be seen from the values of distance and neutral density filter used, there is a much higher intensity value in the central peak for on-axis radiation than for off-axis radiation. This is consistent

with the Strehl Ratio argument from Chapter 3. This also shows that one of the main problems with a large field-of-view is not the addition of side lobes, but the loss of power in the central peak.

Figures 13 and 14 give the results from the computational analyses of the lenses used in the above experiment. The data is normalized to 1 cm per 17 matrix elements. As can be seen, the plots for various values of alpha are consistent with the information obtained from the experiment.

The only aberration to be concerned with for $\alpha = 0$ is spherical aberration. The first lens was of poor quality, an Airy pattern never being achieved using this lens. Therefore this lens exhibits more aberrations, such as astigmatism, than the computations would handle. The experimental results for the second lens are very similar to the results found from the computational analysis for $\alpha = 0$. As the incident angle grew for the first lens, astigmatism became the dominant contributor to the intensity pattern. This occured through an angle of ten degrees. After ten degrees, the dominant contributor became coma and at this point there is a serious problem with the intensity pattern shifting in the image plane. As can be expected from a thicker lens, the results are just a worse case of the first lens. Astigmatism became a problem at an angle of two degrees, and coma became a problem at an angle of five degrees. As can be seen in the last picture for the second lens ($\alpha = 20$), the intensity pattern became so large that the telescope became the limiting aperture. Again, the results from the computational analysis did not have this problem. However, the program's results are not as accurate for this second lens as they were for the first. Also, the matrix size was too small for

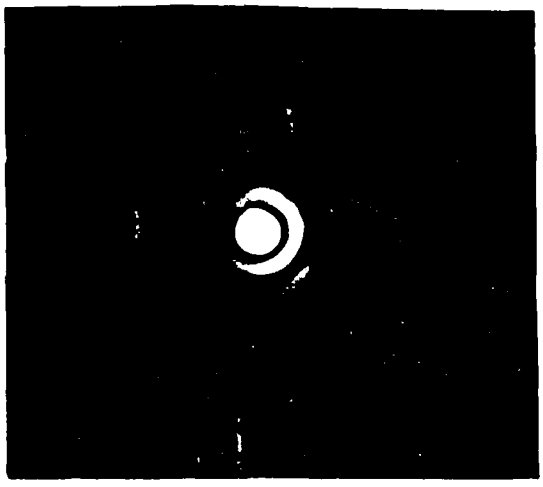

$\alpha = 0$
nd = 2.6
d = 313cm

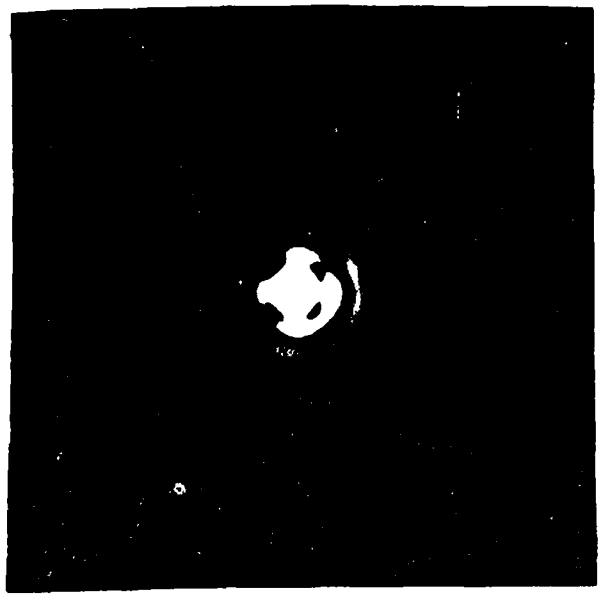

$\alpha = 2$
nd = 2.4
d = 313cm

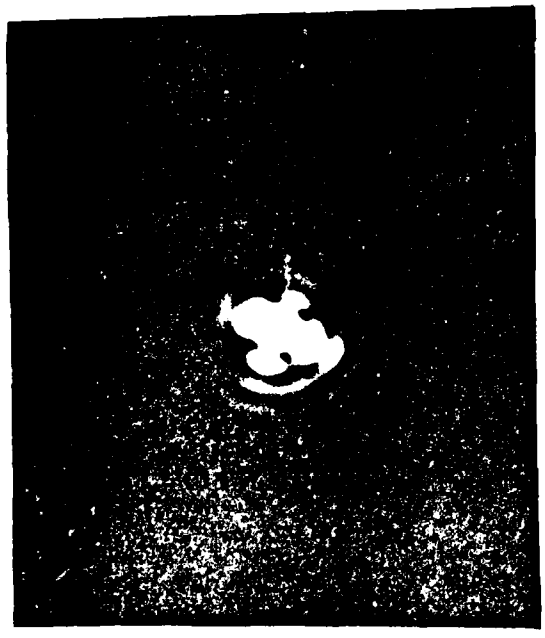

$\alpha = 5$
nd = 2.2
d=313cm

Figure 19a. Experimental Results for Lens 1 at $\alpha = 0$, 2, and 5 Degrees

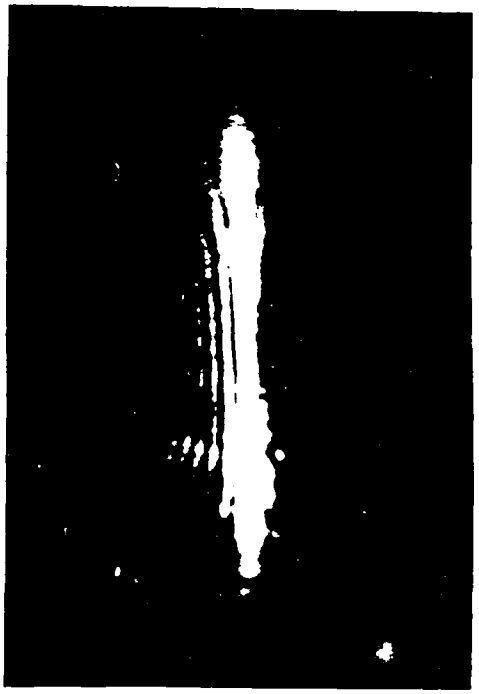

$\alpha = 10$
nd = 2.0
d = 160cm

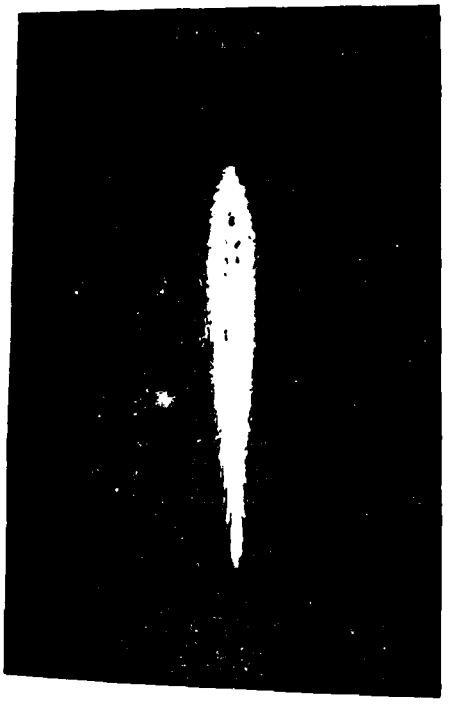

$\alpha = 15$
nd = 2.4
d = 45cm

$\alpha = 20$
nd = 2.4
d = 20cm

Figure 19b. Experimental Results for Lens 1 at $\alpha = 10$, 15, and 20 Degrees

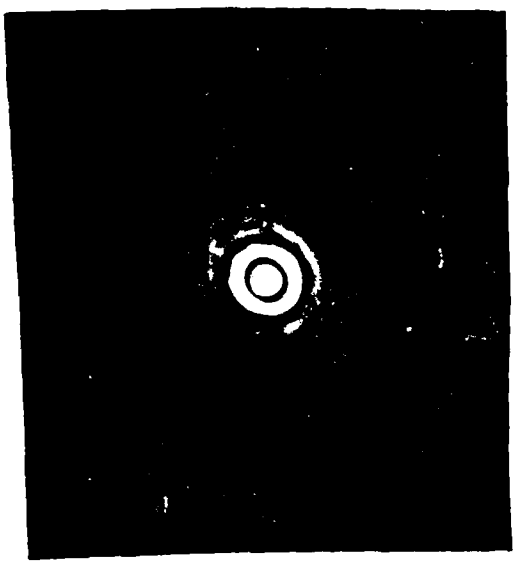

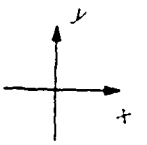

$\alpha = 0$
nd = 2.6
d = 326cm

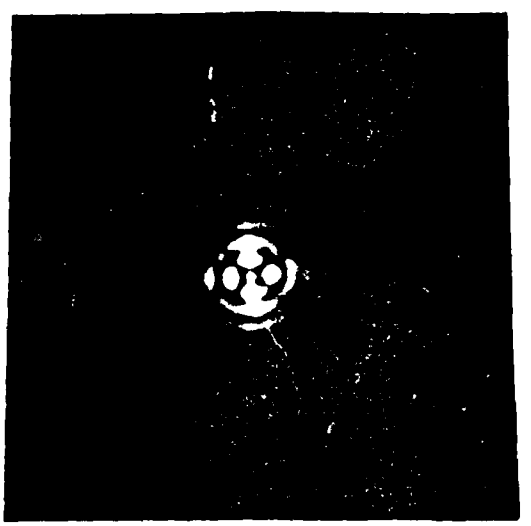

$\alpha = 2$
nd = 3.2
d = 326cm

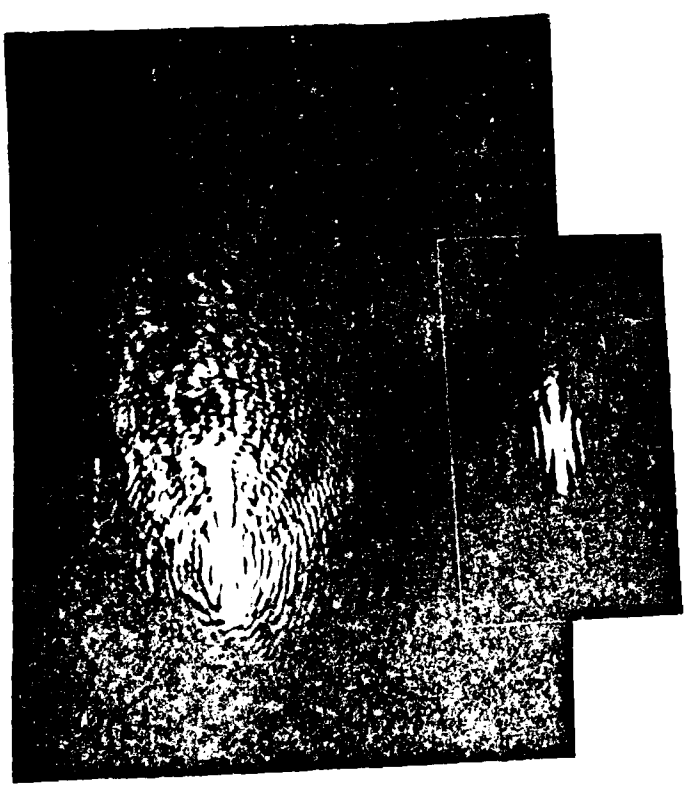

$\alpha = 5$
nd = 2.4
d = 165cm

Figure 20a. Experimental Results for Lens 2 at $\alpha = 0$, 2, and 5 Degrees

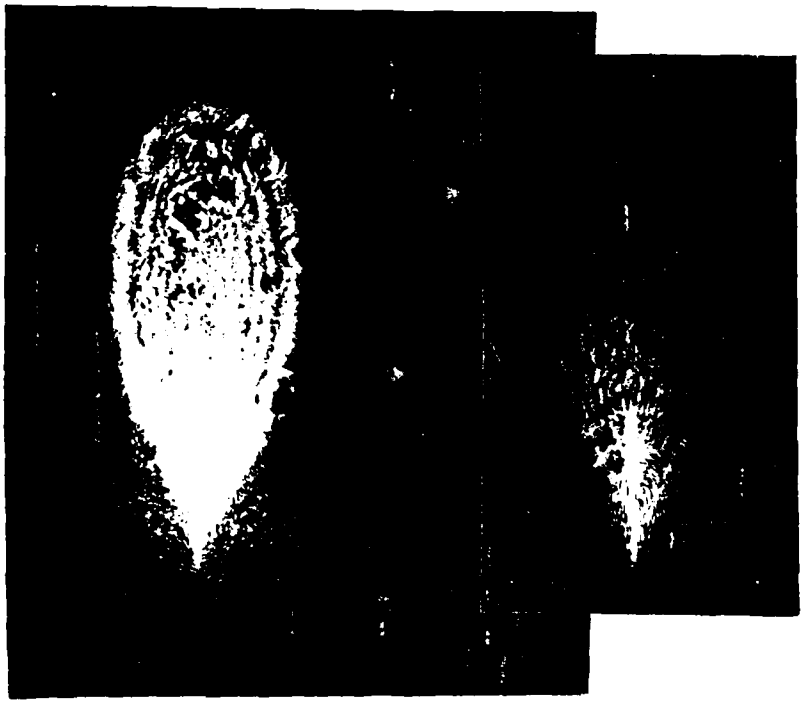

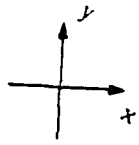

$\alpha = 10$
nd = 2.0
d = 56cm

$\alpha = 15$
nd = 2.4
d = 25cm

$\alpha = 20$
nd = 2.4
d = 16cm

Figure 20b. Experimental Results for Lens 2 at $\alpha = 10$, 15, and 20 Degrees

any results at an angle of alpha greater than ten degrees, so no accurate comparisons can be made between analysis and experiment in this region. In the region $0 < \alpha < 10$ degrees however, there is good correlation, just as had been hypothesized.

Therefore, as has been seen from the experimental results given above. Goodman's analysis is a good approximation for on-axis radiation effects. If Geary and Peterson's term is used, the result becomes extremely accurate for on-axis radiation, but, does not hold for off-axis radiation. The most obvious difference between these previous results and the new expression for the thin lens derived herein is that instead of off-axis effects simply moving the intensity pattern in the image plane, these effects actually do not move the pattern as much as cause deformation of the pattern and severe aberrations for large angles. Although beam deformation does seem to be a problem for the field-of-view required by SDI, the amount of normalized intensity, or power, lost in the central lobe as the angle alpha is increased can also cause serious problems for detection.

VI. Application: Multi-Aperture Systems

In this chapter, muli-aperture systems will be applied to both the thin and the thick lenses investigated previously, and the effect of aberrations on field-of-view will be investigated. Note that in all of the multi-aperture intensity patterns, the envelope of the pattern is the intensity pattern for the single lens used in the system. In all of the following analyses, the optic axis is located at (129,129) and 17 matrix element are taken to be 1 cm. The configurations to be used in this chapter are given in Figure 2. The program written to compute the intensity patterns for the multi-aperture configurations is included in Appendix D.

VI.1. Single versus Multi-Aperture Patterns

Given in Figure 21 are the intensity patterns for the single thin Lens 1 at an angle $\alpha = 5$ degrees and the four aperture case using this lens at an angle of five degrees as well. Note that the pattern for the single lens is the envelope for the multi-aperture pattern. This result is in keeping with the theory as shown by Young (12:281-283) in his classic double slit experiment.

VI.2. Multi-Aperture System Using Goodman Analysis

As a comparison to the previous theory, the Goodman analysis was applied to the three multi-aperture systems given in Figure 2. As can be seen from Figures 22 through 24, as the angle alpha increases to twenty degrees the side lobes

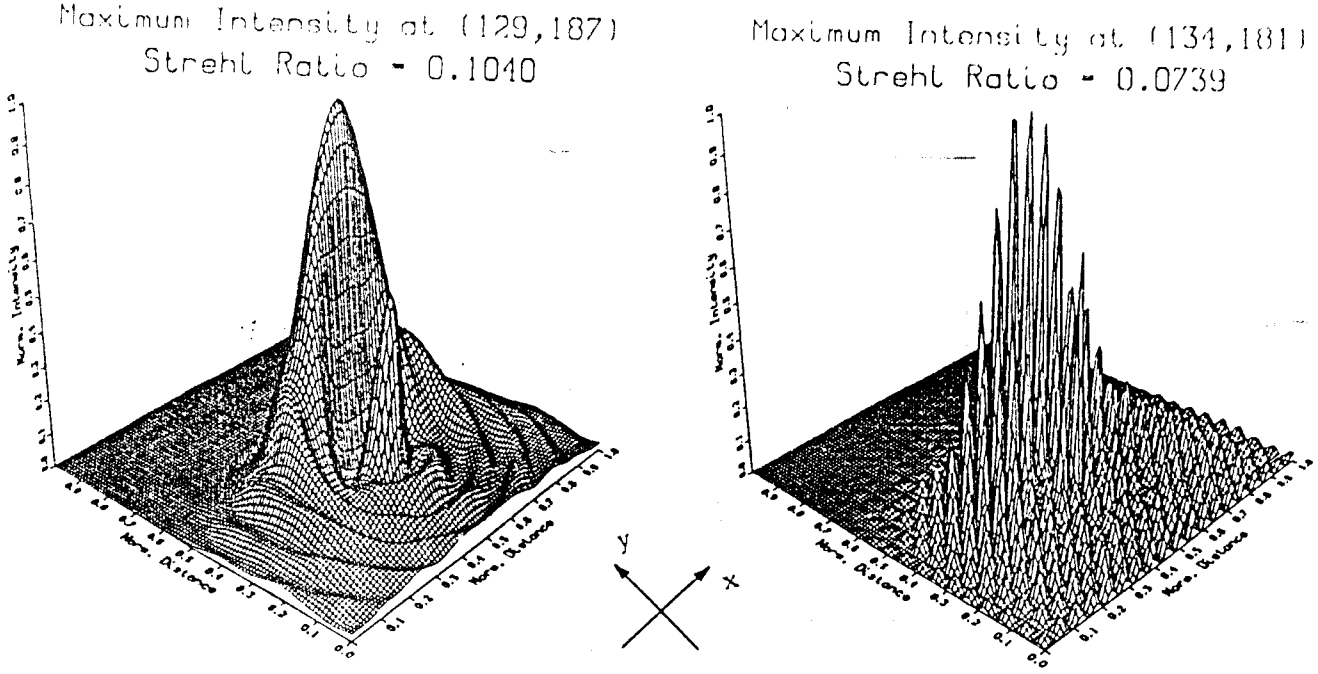

Figure 21. Single vs. Multi-Aperture

grow asymmetrically in the pattern. As the angle increases through ten degrees the side lobes approach a maximum, and as the angle approaches twenty degrees the side lobes decrease again. This phenomenon is apparent in all of the multi-aperture configurations using the Goodman thin lens model. The form of these results are not consistent with standard results using Goodman's thin lens. However, the analyses of interest in this thesis were based on the new lens equation so this discrepency was not investigated. The only lens used in this analysis is Lens 1 since the patterns for this lens and Lens 2 are essentially the same. Note that the Strehl ratios for the Goodman analysis decreased by a finite amount as in the single aperture case. Again, this is due to the effects of spherical aberration and defocus as described in Chapter 4.

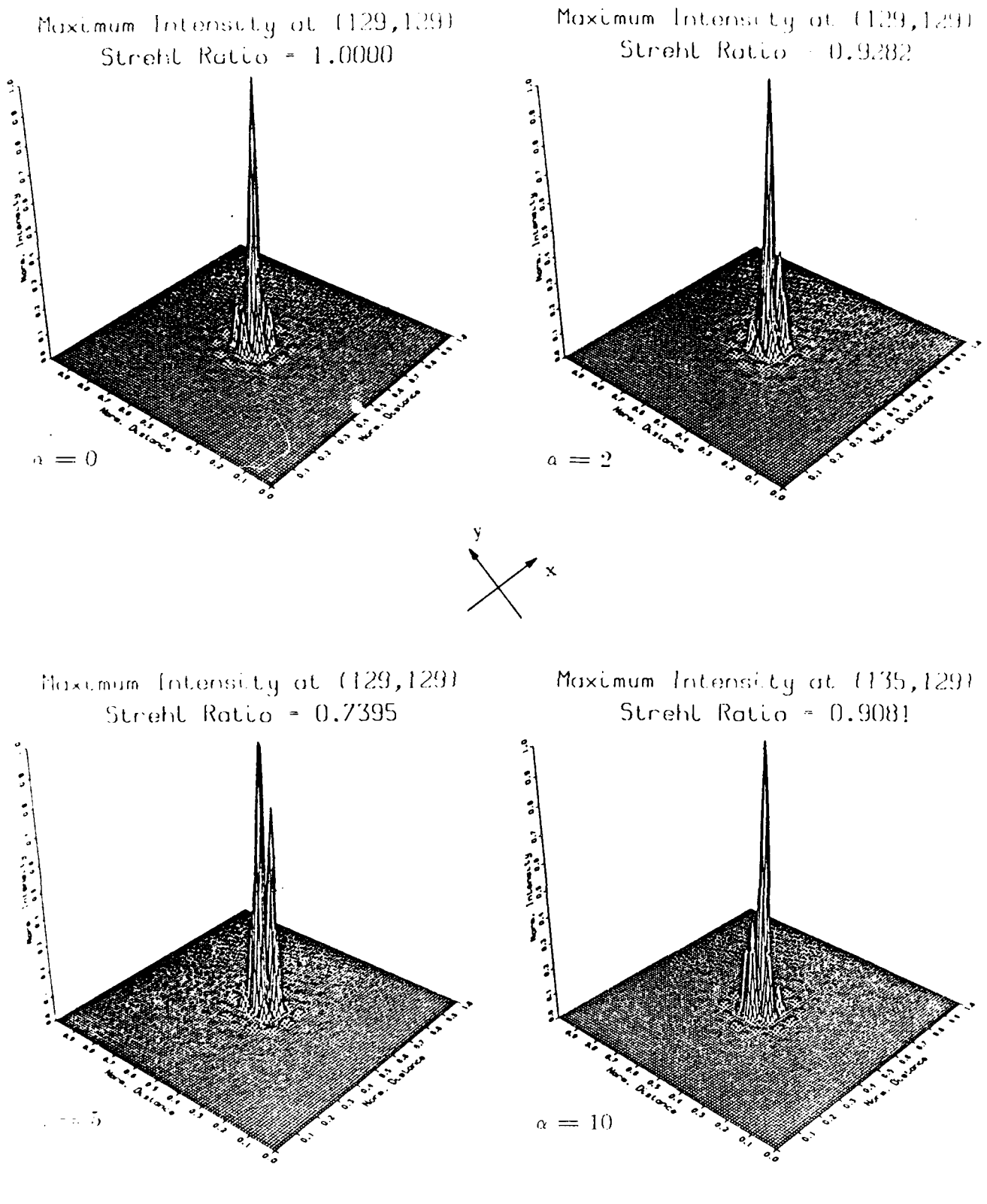

Figure 22. Goodman Lens 1 in Three Aperture Configuration

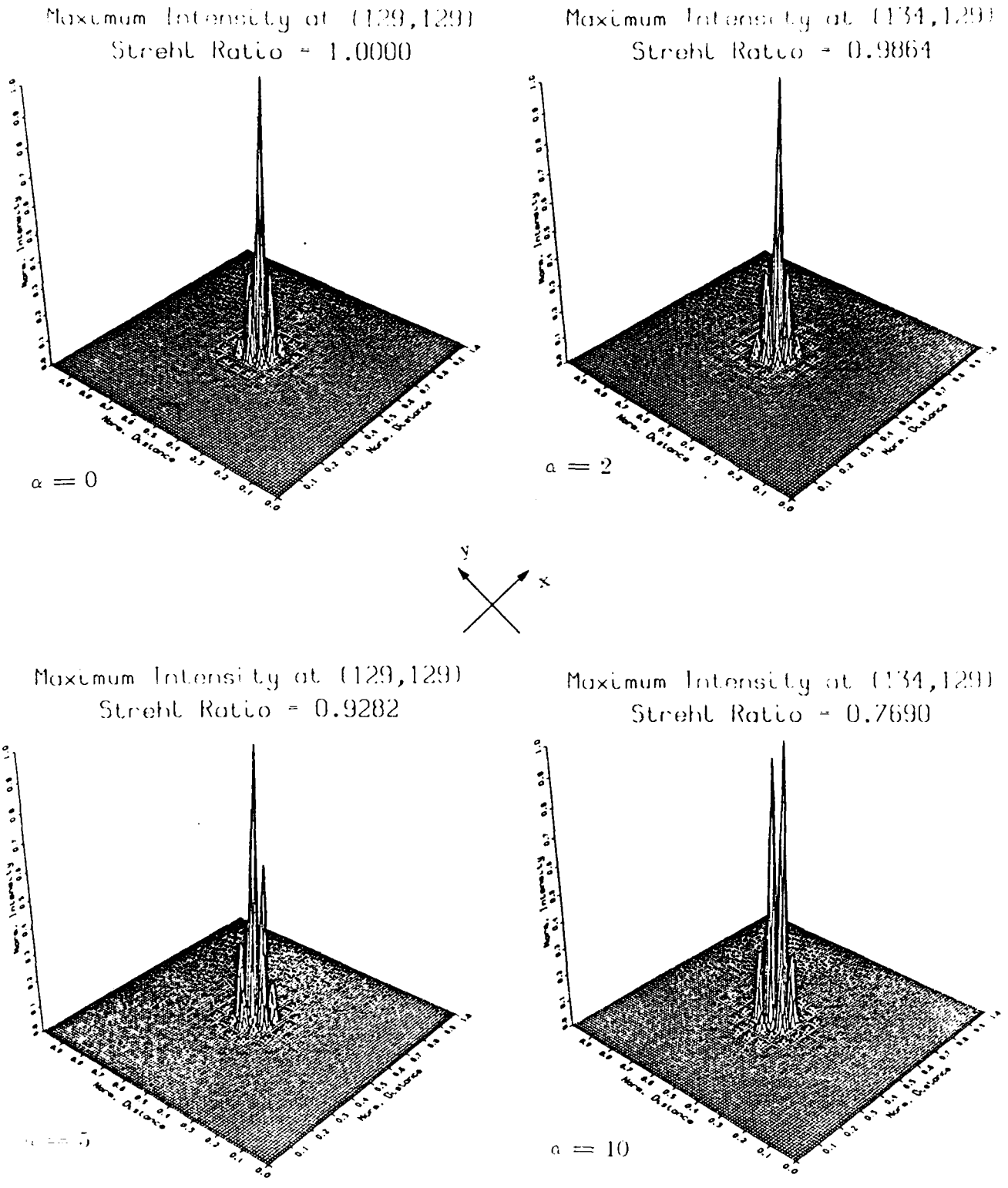

Figure 23. Goodman Lens 1 in Four Aperture Configuration

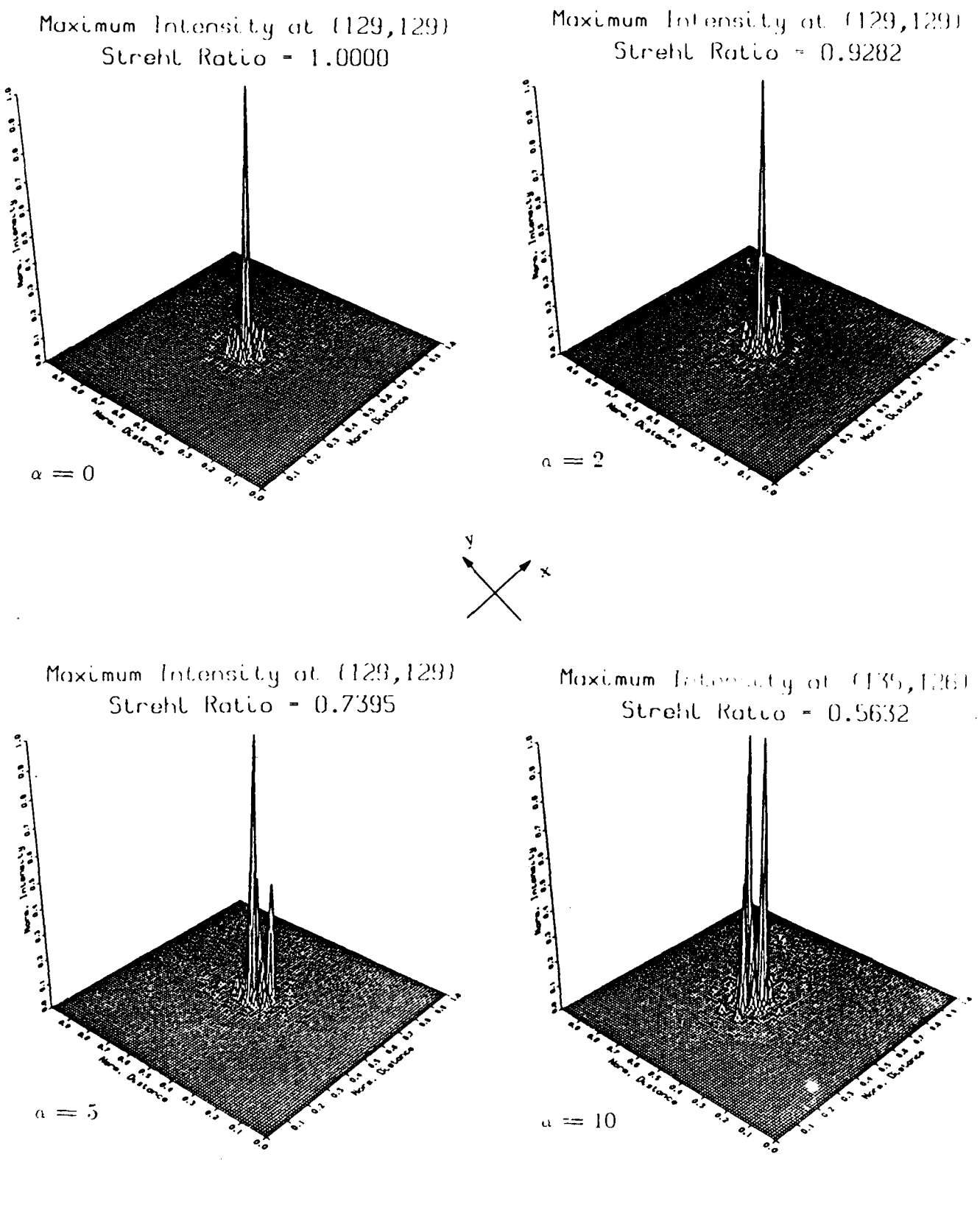

Figure 24. Goodman Lens 1 in Six Aperture Configuration

VI.3. Three Apertures

The following analysis is for Lens 1 and Lens 2 in the three aperture configuration. Given in Figure 25 and Figure 26 are the graphs for the intensity patterns at various values of alpha for both lenses. As can be seen from Lens 1, the central peak is much more narrow than for the single lens case. Therefore, two point resolution for multi-aperture systems is much better than for a single lens as has been reported previously (5:40-46). However, as the incident radiation impinges the lens at an angle greater than zero, the side lobes on one side of the central peak grow more than those on the other side. This is apparent from the intensity patterns for the single lens which form the envelope for these plots. At angles larger than five degrees coma is the dominant aberration, which causes an asymmetric shift of the light intensity to one side of the pattern. Thus, there is consistency with patterns shown in Figures 13 and 14 and the information given above. As the angle of incidence grows to five degrees, the side lobes grow to approach the height of the central peak. In addition, there is a small shift in the x axis caused by astigmatism which has to be included. This causes problems with detection which has not been dealt with in any of the research to date. However, with any kind of threshold level detector this problem can be overcome (5:63-64). From the graphs in Figure 25, as alpha grows, the main lobe separates into many peaks, causing definite problems for two point resolution as pointed out by Watson (5:40-62). An additional problem for this optical system is that the amount of power in the central peak at an angle of five degrees is approximately 10 percent of that in the $\alpha = 0$ case.

Lens 2, as seen in Figure 26, is a poor lens based on multi-aperture considerations. At an angle of zero degrees, the side lobes of the system are approximately 45 percent of the intensity of the central peak. This is obviously not a good multi-aperture system. As the angle grows, the side lobes increase to the point that by the time the angle is two degrees, the side lobes are within 90 percent of the central peak. At an angle of ten degrees the central intensity begins to walk down the x as well as the y axis. Again, this must be accounted for in the detection system. For angles above two to five degrees, virtually no information can be gleaned from this system with the thick lens because of the many peaks in the central region. In addition, the central intensity has decreased to approximately one percent of its initial value. The aberrations present as the angle increases indicate that this lens is unacceptable for multi-aperture systems.

VI.4. Four Apertures

In Figure 27 are the intensity patterns for the four aperture system at various angles alpha. The four apertures almost completely fill a square in the optical system, thus a square pattern is achieved in the image plane. The multi-aperture intensity plots for Lens 1 are much better than for Lens 2 based on the results from section VI.3. Therefore, the analysis of Lens 2 for the four aperture case will be omitted. For Lens 1, the side lobes are very small at $\alpha = 0$. However, as the angle approaches two degrees, the side lobes are approximately 85 percent of the central peak intensity. Again, as the angle alpha increases, the number of peaks in the same range as the central maximum increase, and thus there are problems

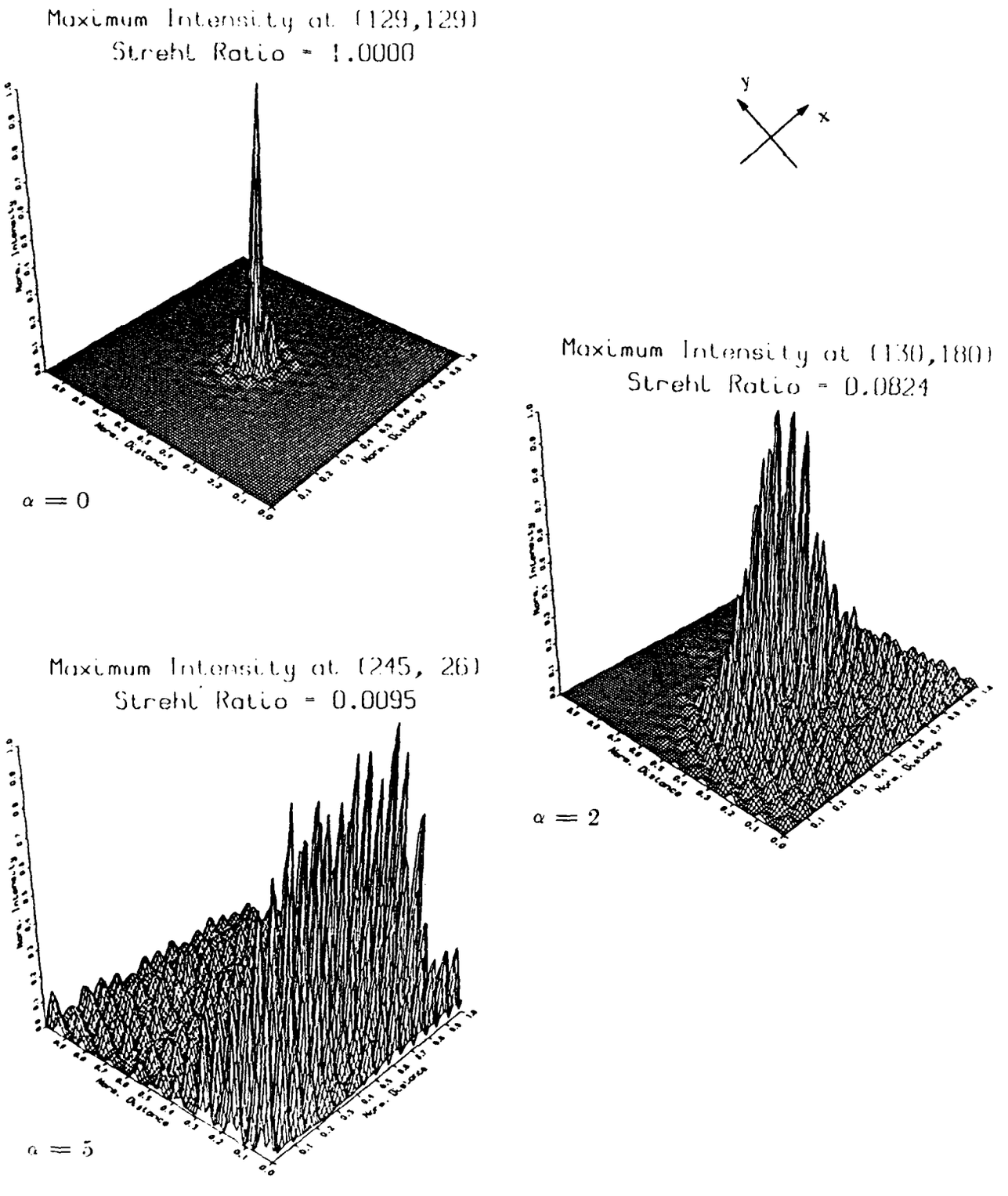

Figure 25. Walton Lens 1 in Three Aperture Configuration

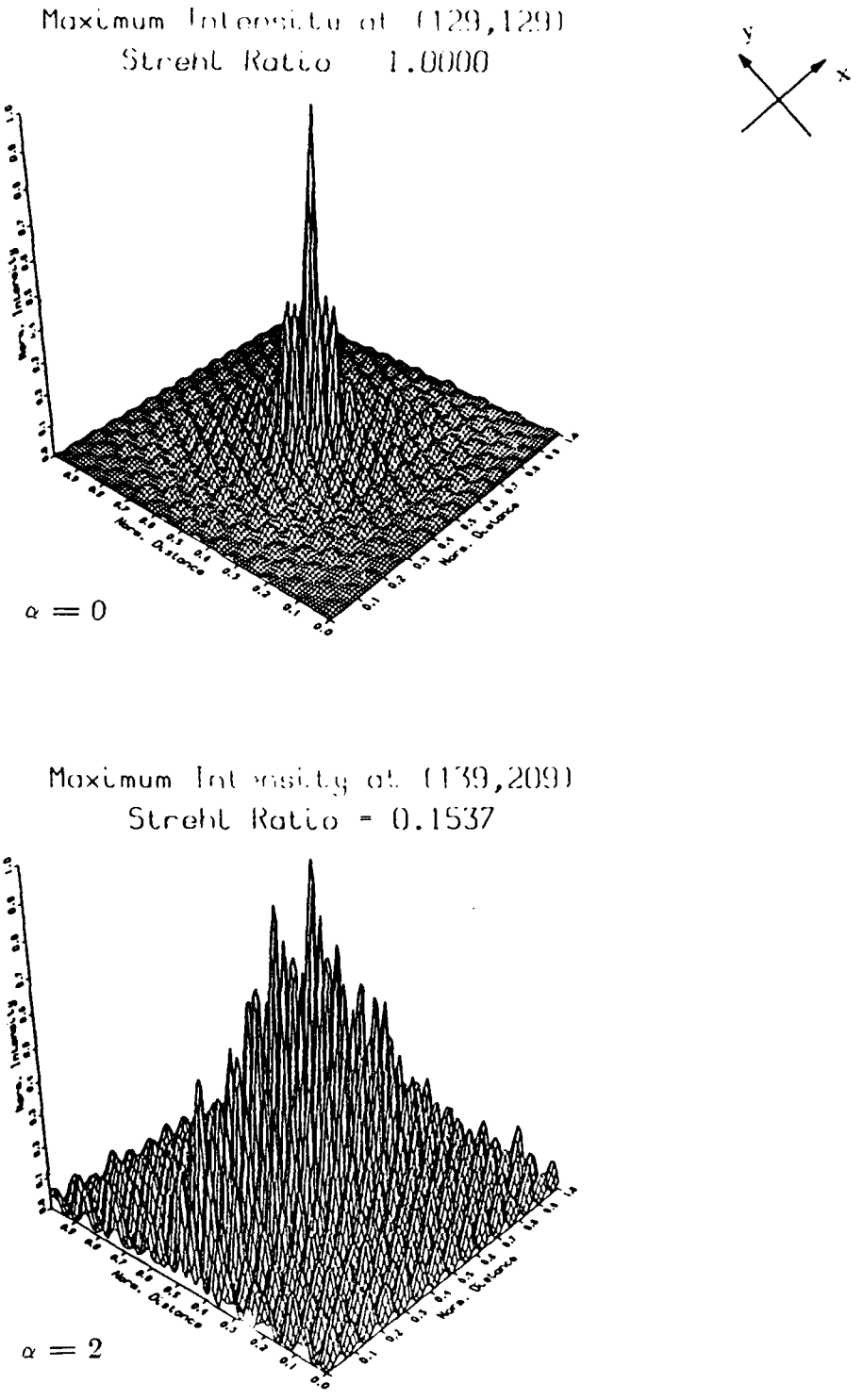

Figure 26. Walton Lens 2 in Three Aperture Configuration

with a large field-of-view for this system. As before, the central peak shifts down the x axis, by a relatively small amount compared to the shift down the y axis.

VI.5. Six Apertures

Figure 28 gives the intensity patterns for the six aperture system at various angles alpha. As can be seen from the patterns for Lens 1, the central peak has decreased in width significantly from the three aperture case, and the side lobes are also much smaller than in any of the previous systems. These are excellent results based on two point resolution criteria. However, as the angle alpha grows, many side lobes increase to a height equivalent to the central peak by an angle of five degrees. This optical arrangement actually proves to be a far worse configuration than that for the three aperture case. This result contradicts previous research (5,6). Therefore, this optical system shows the same problems as the previous two optical systems. This is an unexpected result based on previous research concerning SDI's required twenty degree field-of-view. No comment will be made about the six aperture case for Lens 2 given the results from the three aperture case.

VI.6. Field-of-View and Power Considerations

Field-of-view and power in the central peak are the two basic problems of interest within this thesis. As can be seen from Figures 25 through 28, the field-of-view of any system varies with the number of apertures in the system, their

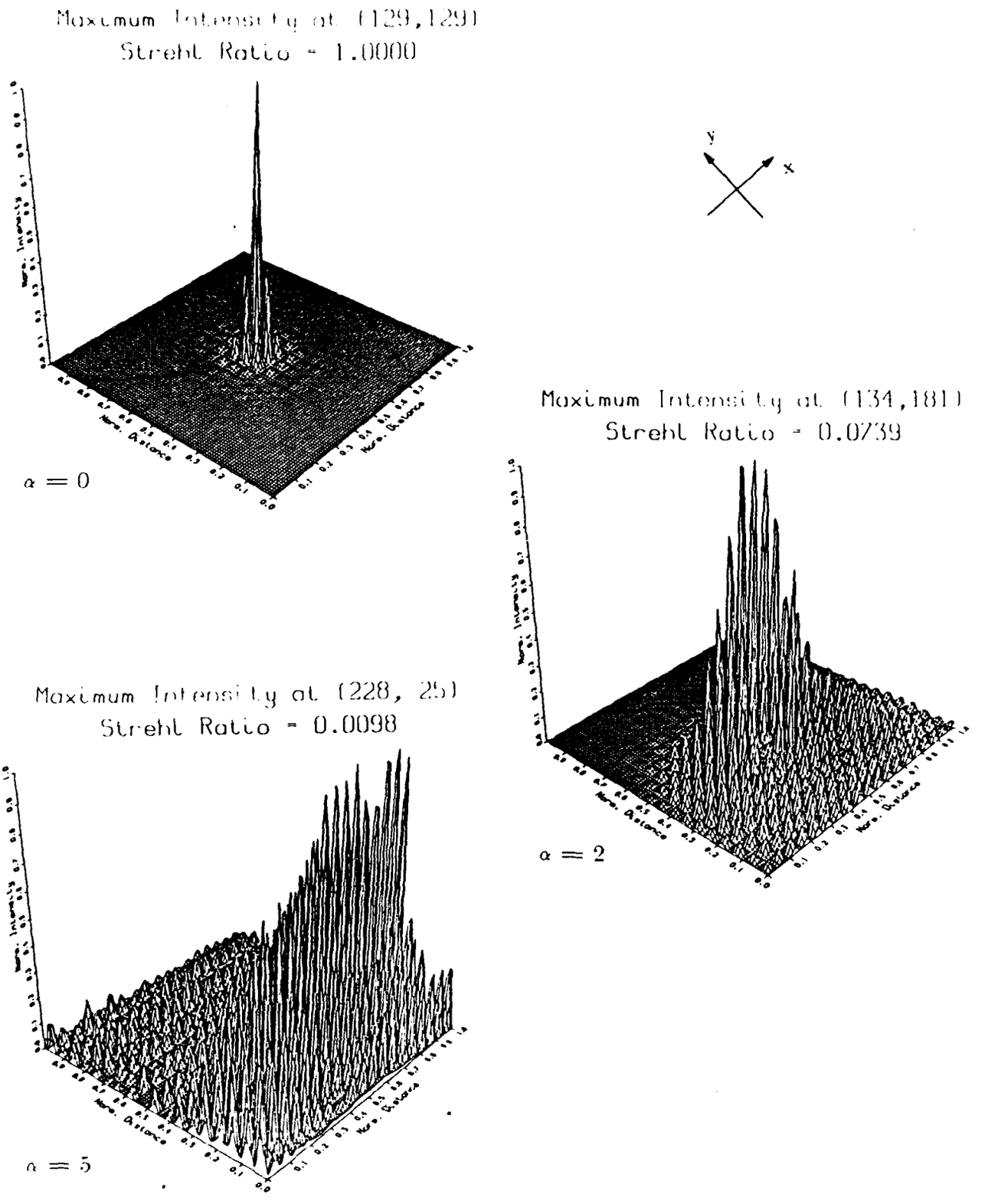

Figure 27. Walton Lens 1 in Four Aperture Configuration

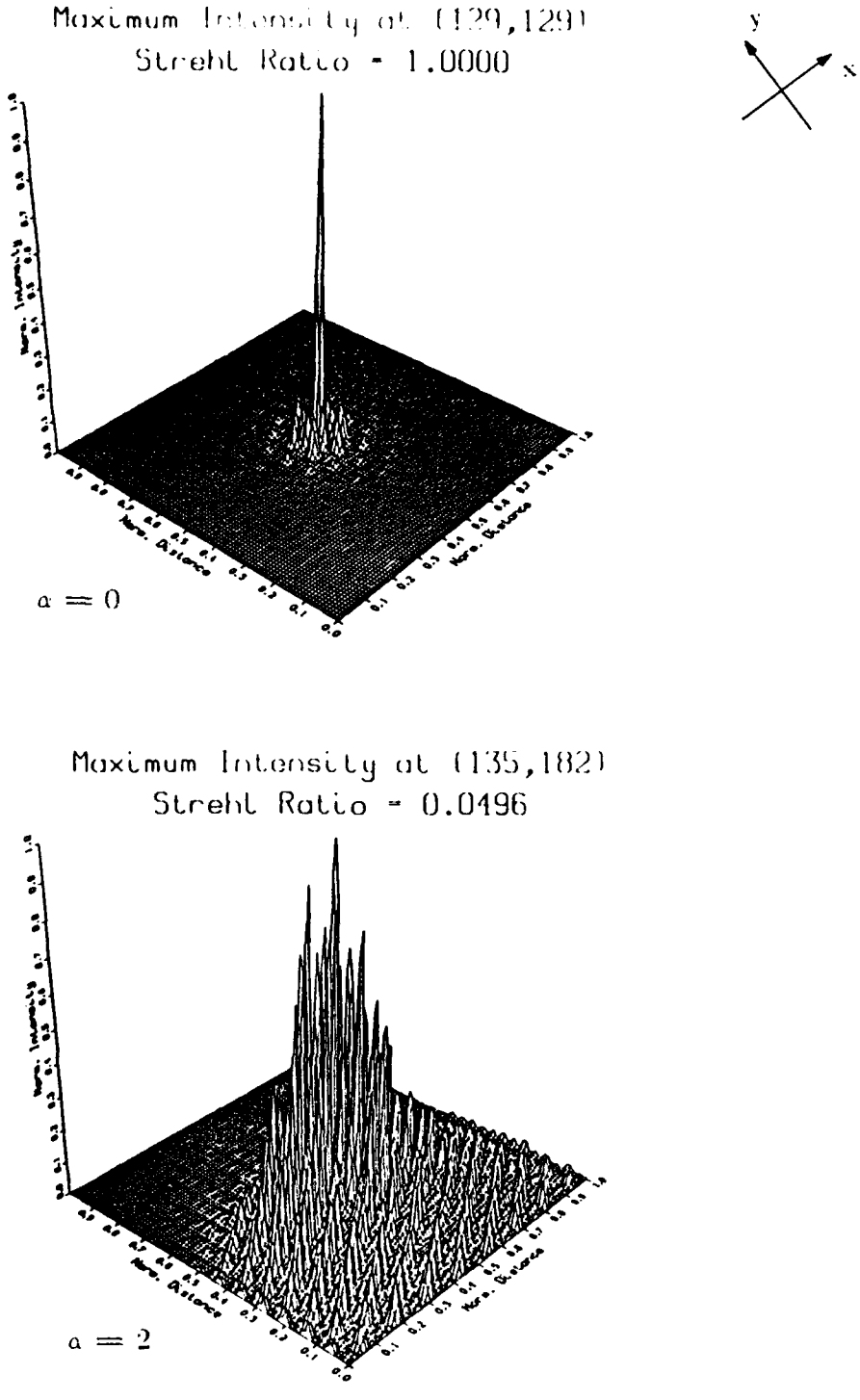

Figure 28. Walton Lens 1 in Six Aperture Configuration

placement, and the angle of incidence of the incoming radiation. Only Lens 1 will be considered in this synopsis since the intensity patterns for Lens 2 were so poor when compared to Lens 1. As determined previously, the more apertures there are in the optical system, the narrower the central peak, which is a very good result for two point resolution. Also aperture placement is important in field-of-view considerations. While the four aperture case was poor when compared to the three aperture case, the six aperture case seemed to be the best of all systems studied. However, this is apparently only for on-axis radiation. The computations achieved in this thesis indicate that for off-axis radiation with a more accurate analysis for the transfer function of a thin lens, the beam degradation actually becomes far worse as the number of apertures is increased. Also, there exists a problem of threshold levels dependent upon the angle of incidence. At angles less than five degrees these systems behave well, but for angles greater than five to ten degrees the system performance degrades due to the large number of side lobes of the same approximate size as the central peak. The structure of these patterns, i.e. the envelope, is the same as that obtained in the experiment.

The main problem forseen in future optical systems is not the problem of field- of-view in relation to two point resolution but the problem that the further off-axis the incident radiation, the le power appearing in the central lobe. This could cause serious problems with tection as has been mentioned previously. If insufficient intensity exists to detect the signal, aberrations are essentially unimportant. Also, if any kind of threshold system were used for this detector, the angle of incidence must be considered so that the threshold could be varied. This poses an extremely difficult design problem for future optical systems.

VII. Results: A Comparison of the Four Methods

Given in this chapter is a comparison of the four analyses discussed previously to find an overall method for describing a transfer function of a thin lens appropriate for off-axis projections. The four methods discussed are: Goodman's Analysis, The Walton Analysis, FALCON, and Experiment.

VII.1. Comparison of the Results

Given in Figures 29 through 32 are a comparison of the results at the specific angles zero, two, five, and ten degrees for Lens 1. At zero degrees, all four of the methods correlate extremely well. This is the limiting condition for the Walton analysis, and the validity regime for the Goodman analysis. This result is excellent since it shows consistency with the results shown previously in the literature (1,8). The only aberration present in this analysis is spherical aberration.

At an angle of two degrees, the Goodman analysis shows that there is no beam deformation, only a translation in the y axis from the plane wave. However, the experiment explicitly shows how astigmatism is present as well as a small translation in the y axis. FALCON shows not only an astigmatic problem, but also a contribution due to coma. The Walton analysis shows the same intensity distribution as the experiment.

At an angle of five degrees, the Goodman analysis again shows only a translation in the y axis. The experiment shows not only an astigmatic problem, but a

large contribution due to coma. The intensity distributions from FALCON show only the portion of the coma pattern in the y direction, the point of maximum intensity. The Walton analysis at this point shows not only the portion of the coma pattern in the y direction, but the astigmatic asymmetry in the x direction as well. The Walton analysis correlates well with the experimental results.

At an angle of ten degrees, the Goodman analysis shows a further translation. The experimental result shows a large component due to coma, which literally washes out the comtribution due to astigmatism. The FALCON analysis has exceeded the limitations of the program because of the finite size of the matrix used in the FFT. The Walton analysis again correlates well with the experimental results.

Given in Figures 33 through 36 are the results for Lens 2. The analysis is the same as that of Lens 1 except that the strength of the aberrations occur at much smaller angles than for Lens 1. Also, the Walton analysis has broken down since a thick lens does not agree with the basic assumption of the analysis. FALCON, as before, breaks down after five degrees since the analysis has exceeded the limitations of the program.

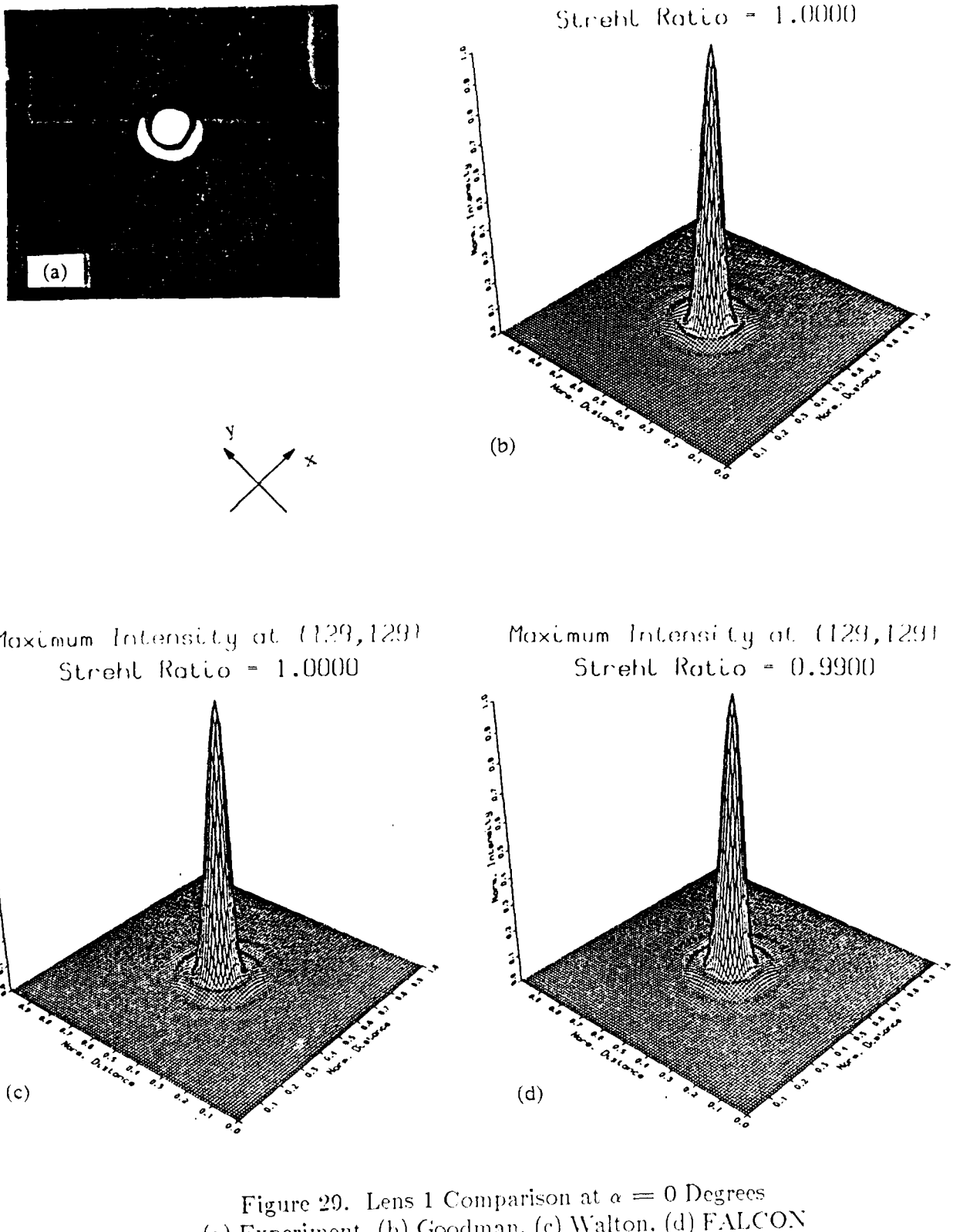

Figure 29. Lens 1 Comparison at $\alpha = 0$ Degrees
(a) Experiment, (b) Goodman, (c) Walton, (d) FALCON

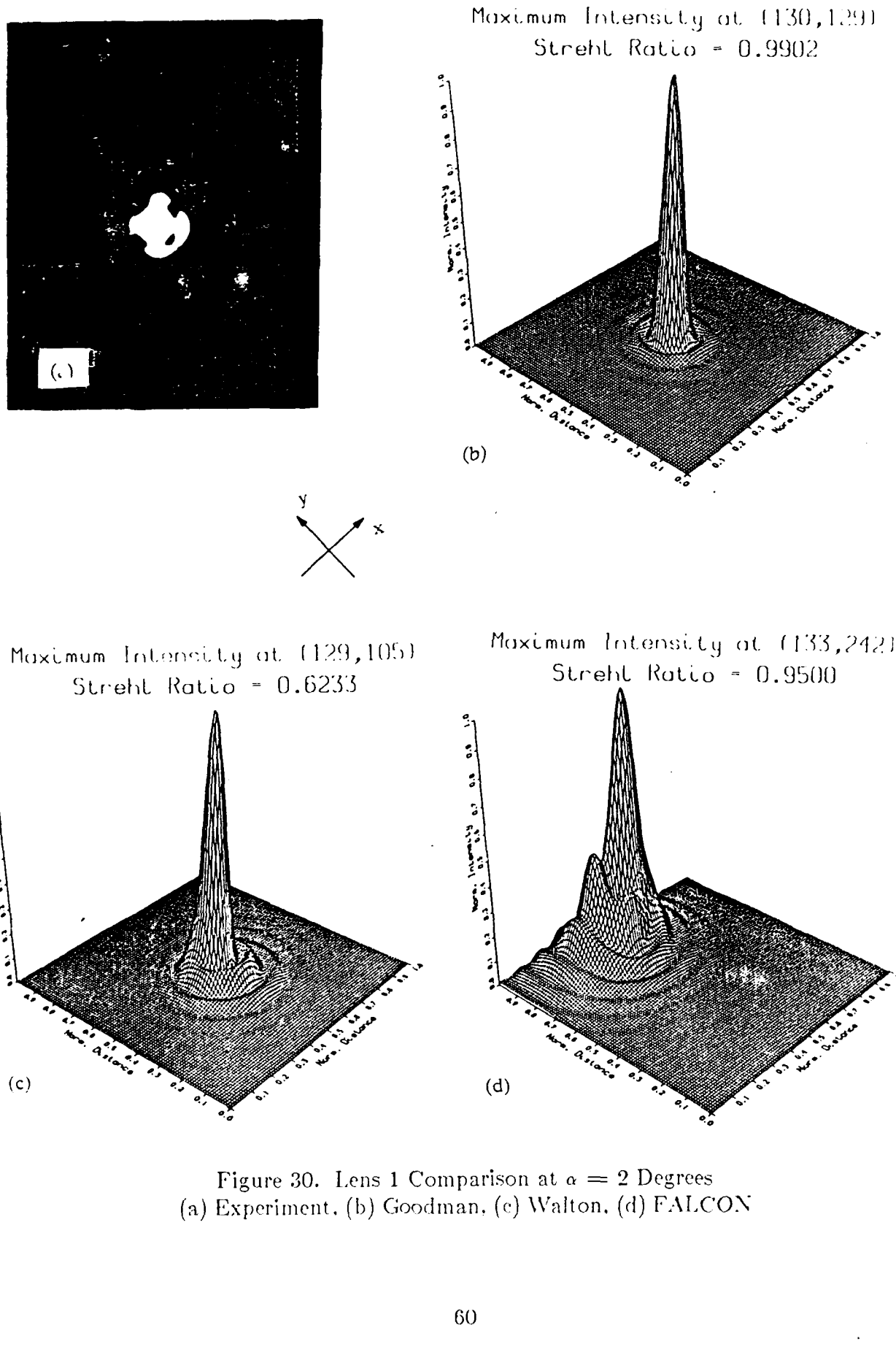

Figure 30. Lens 1 Comparison at $\alpha = 2$ Degrees
(a) Experiment, (b) Goodman, (c) Walton, (d) FALCON

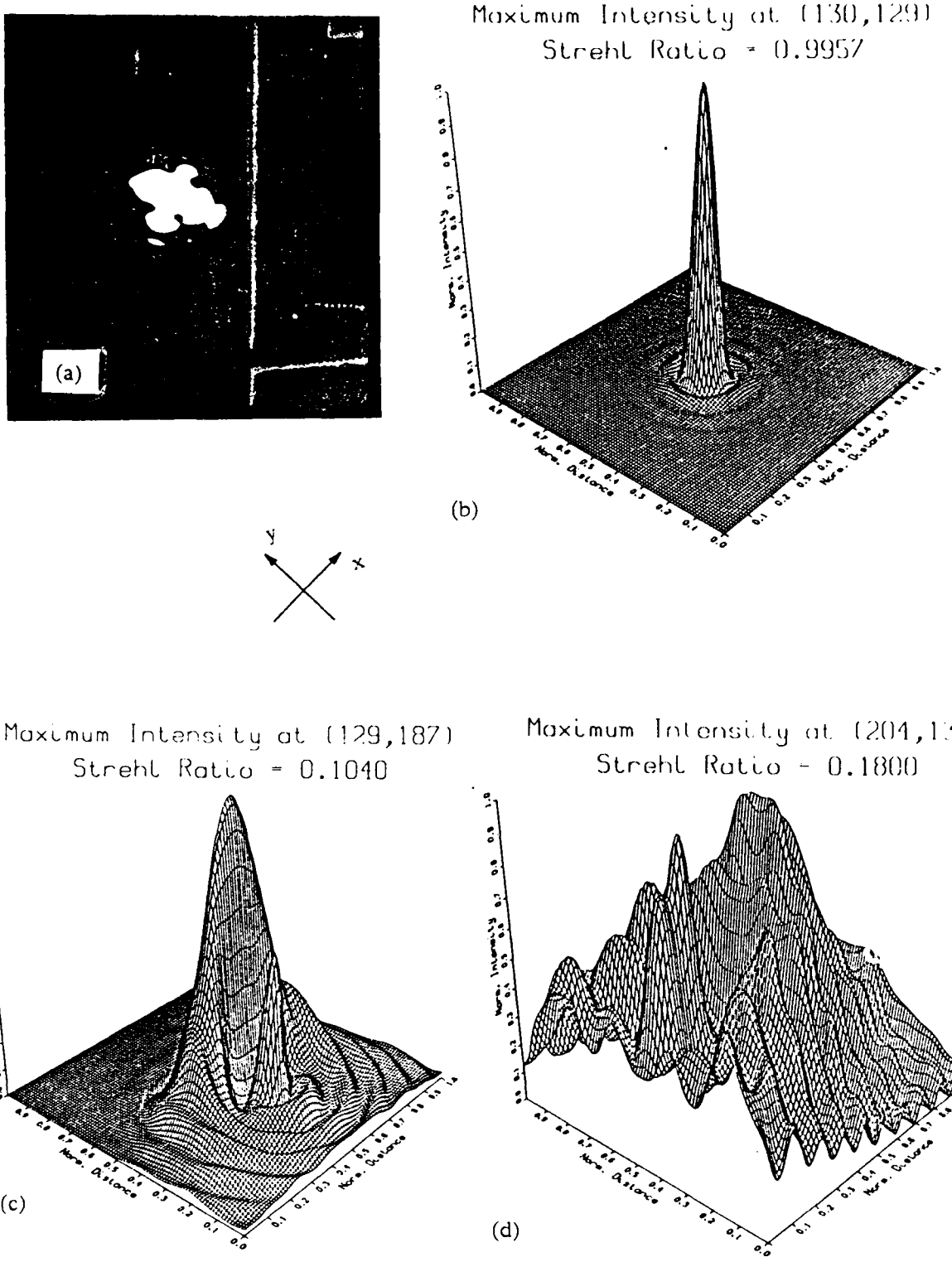

Figure 31. Lens 1 Comparison at $\alpha = 5$ Degrees
(a) Experiment, (b) Goodman, (c) Walton, (d) FALCON

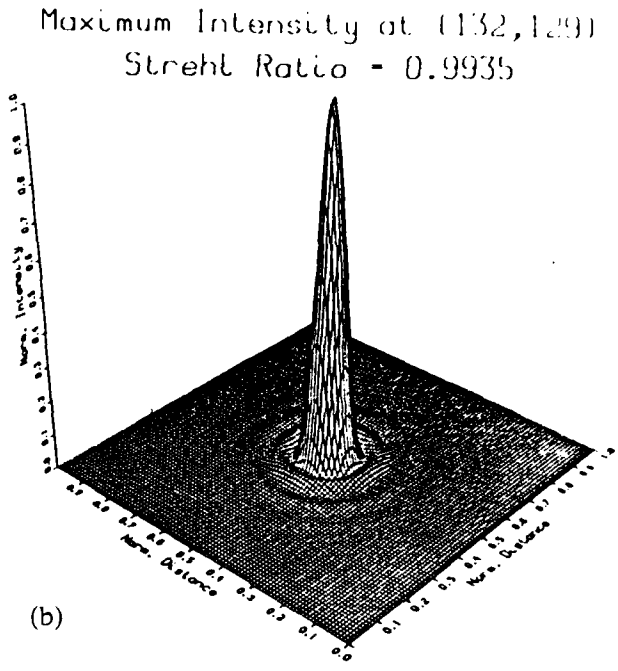

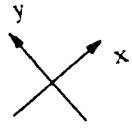

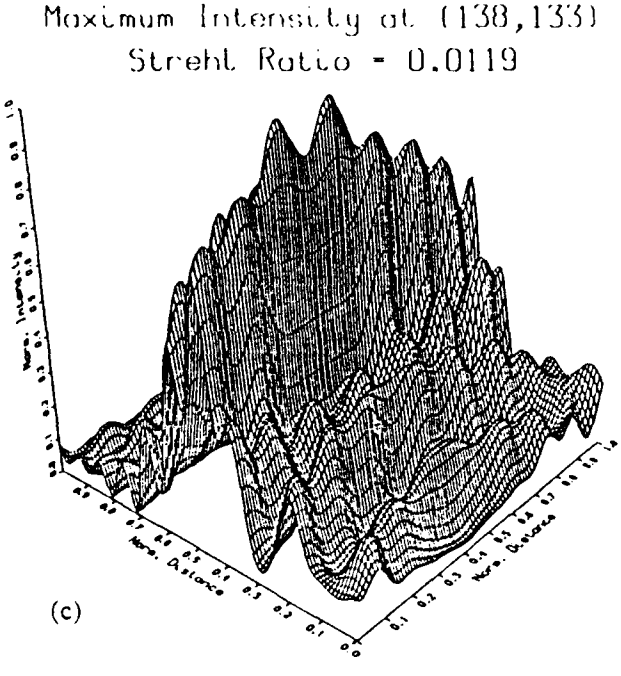

FALCON plot not included due to matrix limitations.

(d)

Figure 32. Lens 1 Comparison at $\alpha = 10$ Degrees
(a) Experiment, (b) Goodman, (c) Walton, (d) FALCON

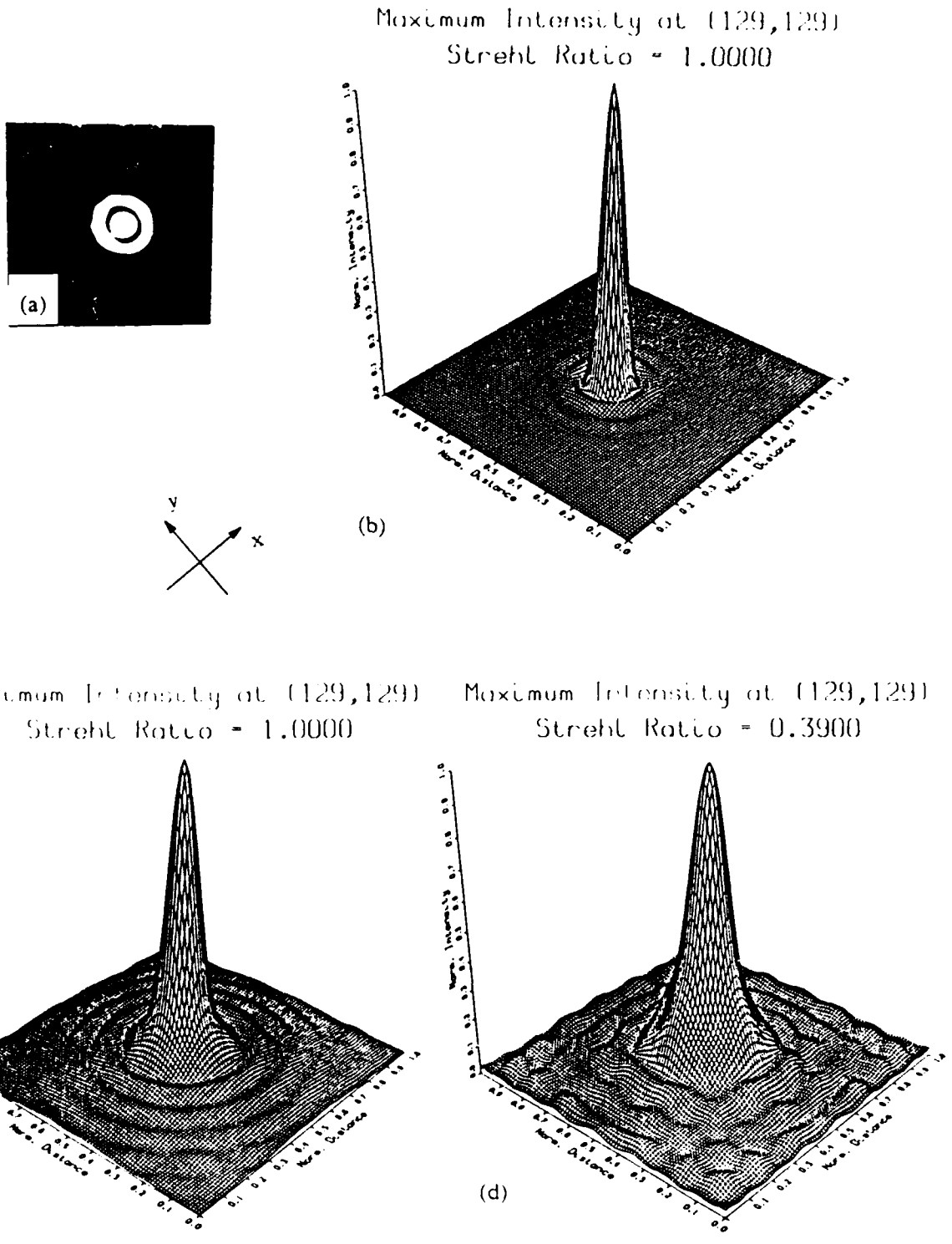

Figure 33. Lens 2 Comparison at $\alpha = 0$ Degrees
(a) Experiment, (b) Goodman, (c) Walton, (d) FALCON

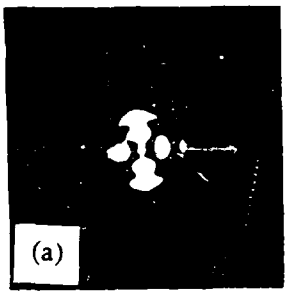

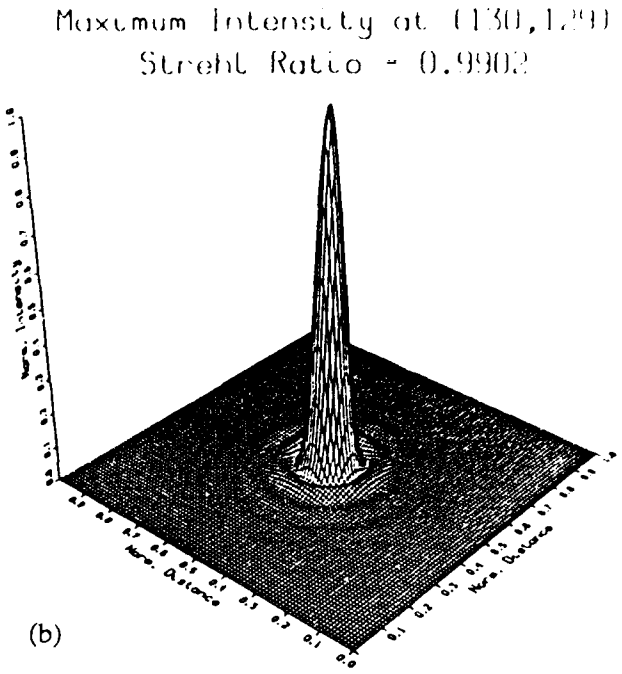

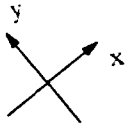

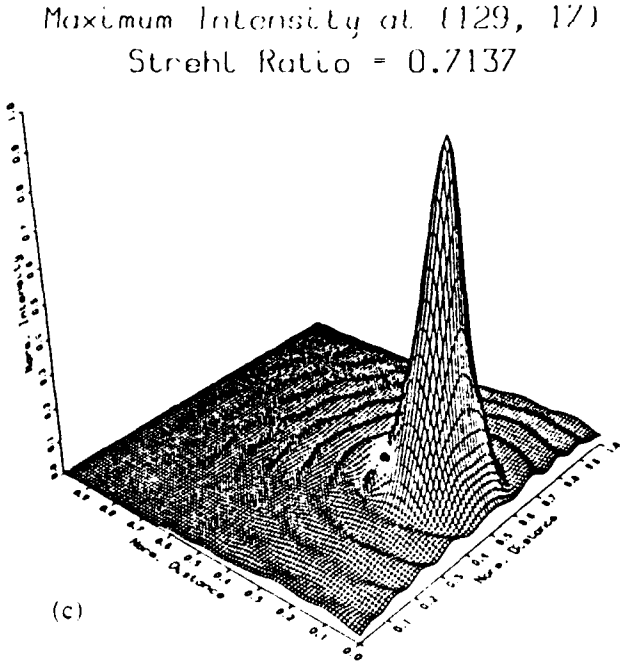

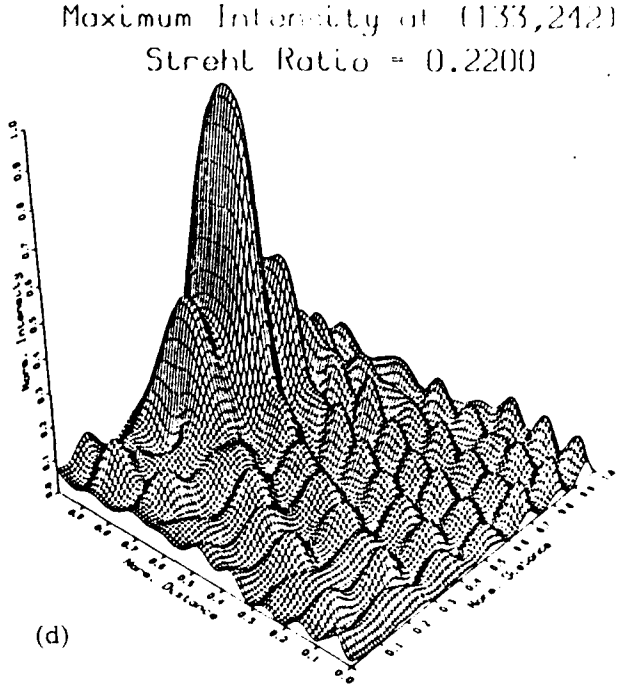

Figure 34. Lens 2 Comparison at $\alpha = 2$ Degrees
(a) Experiment, (b) Goodman, (c) Walton, (d) FALCON

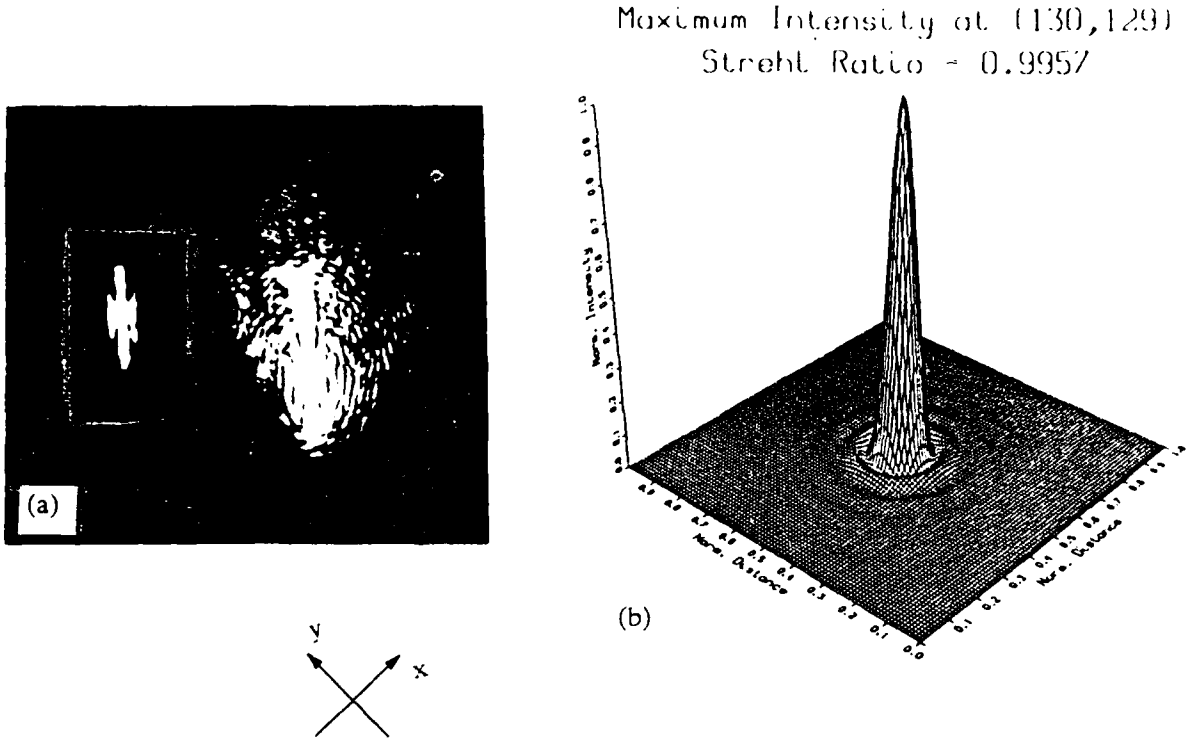

Figure 35. Lens 2 Comparison at $\alpha = 5$ Degrees
(a) Experiment, (b) Goodman, (c) Walton, (d) FALCON

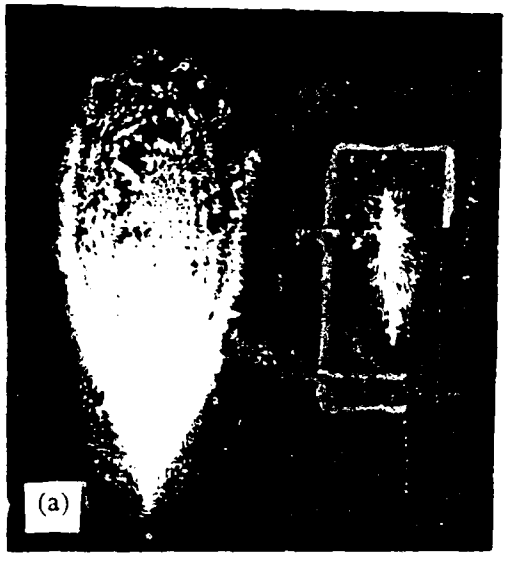

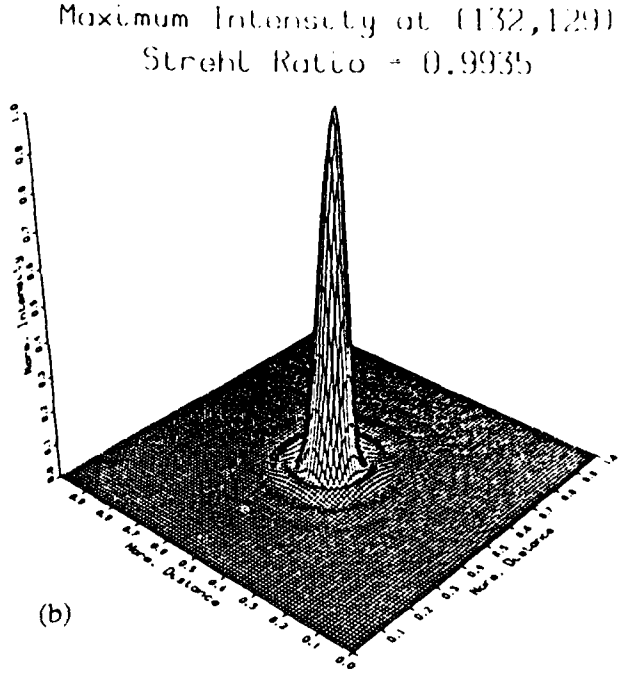

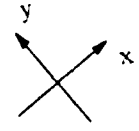

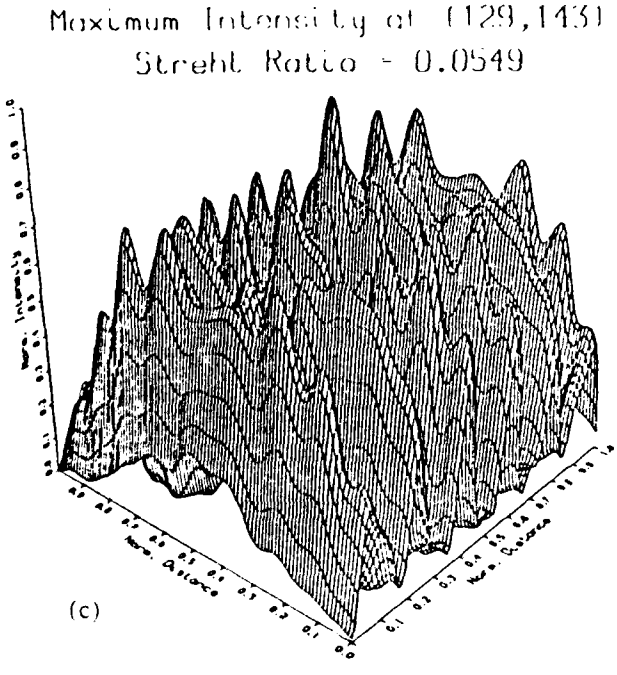

FALCON plot not included due to matrix limitations.

(d)

Figure 36. Lens 2 Comparison at $\alpha = 10$ Degrees
(a) Experiment, (b) Goodman, (c) Walton, (d) FALCON

VIII. Conclusions

This thesis contains a number of breakthroughs, the most important of which is a new expression for a thin lens applicable for off-axis projections. This expression qualitatively analyzes the aberrations induced as the incident radiation impinges a lens at an arbitrary angle alpha with respect to the optic axis. This expression, unlike Goodman's (1:80), displays how the resulting aberrations will affect the field-of-view of a system. This system was verified through various methods, the most important of which was a simple experiment. This experiment explicitly shows how the beam deformation in the image plane affects the field-of-view of an optical system. Through this experiment, the accurate modelling of the system by a computer program was determined.

Subsequently, the program ALPHA was used to model two different lenses, one thin and one thick. The thick lens was employed to test the limitations of the underlying approximations. This lens accurately verified the extent of the thin lens approximation. As the angle alpha grew, the finite limitation of the matrix size in the program limited the field-of-view of the results derived from the Walton analysis.

The thin lens behaved very well, both in the experimental analysis, and under the computational analysis. This lens showed accurately both the problems and results of increasing the angle alpha. As the angle was increased from zero to five degrees, astigmatism became the dominant aberration. As the angle was then increased from five to ten degrees, astigmatism was still present, but coma became

the dominant aberration. Both of these aberrations are off-axis aberrations as defined by Born and Wolf (8:211-218). At an angle of zero degrees, the only aberration present was spherical. The amount of spherical aberration present stayed basically constant as the angle was increased.

The most important result of this thesis is the application of this lens expression to the multi-aperture configurations listed in Chapter VII. These results are very important for SDI initiatives. A field-of-view of twenty degrees is possible from any multi- aperture system made up of thin lenses. However, the number of lenses, placement of the lenses, and the angle of incidence of the incoming radiation are vitally important criteria when designing the most accurate optical system. The more apertures the better the field-of-view for on-axis radiation. However, for off-axis radiation, as alpha increases, the fewer apertures the better for field-of-view considerations. By comparing the three and four aperture case, the placement of the lenses is seen to be a dominant factor in determining the optimum multi-aperture design. Conversely, in all three systems modelled, there was a problem in the image plane of the side lobes approaching the height of the central maximum at angles of incidence between eight and twelve degrees for the Goodman analysis. Further research should be done in this area to ascertain the problems inherent in this angular range of incident radiation based on this specific type of analysis.

The most important result of this thesis is that while the system field-of-view is a significant problem, the power lost in the central maximum is the largest obstacle to overcome. As the incident angle approached ten degrees, the power in the

central peak decreased to one percent of the power in the on-axis case.

A possible solution to this aberrational problem lies in the engineering of the overall optical system. If a beam steering optic, such as a grating, were placed in the optical path of the incident radiation before the first optical element of the receiver it could possibly alter the path from off-axis to on-axis. This would enable the system to use the best imaging criterias of a multi-aperture system while keeping the advantages of an optical beam steering device. More research should also be conducted in the arenas of: the application of incoherent light to the new expression for the thin lens, the effects of off-axis projection within the angles of eight to twelve degrees in the Goodman multi-aperture analysis, and the design of accurate multi- aperture systems incorporating this new lens expression.

APPENDIX A

This appendix contains the code for the program GOODMAN. This program calculates the far-field intensity pattern of the impulse response for the Goodman thin lens at various angles of incident radiation (with respect to the optic axis). The aperture is defined by the knowns: the two radii of curvature for the lens, the radius of the aperture stop, and the angle of incidence α. The various distances through the lens are then calculated for various x and y coordinates in the central plane of the lens as is defined in Figure 4. These distances are then computed as phase lags for the incident plane wave (at an arbitrary angle). This aperture is then Fresnel propagated to the image plane where the intensity plots are computed and given in the text. The parameters, as well as other dimensions determined by the computer, are in units of pixels. The optic axis is centered on the position (128.5,128.5) in the object plane, and in the image plane the system rounds the optic axis to be at the position (129,129).

```
C
C
C     PROGRAM:  GOODMAN.F
C
C
C       THIS PROGRAM CALCULATES THE INTENSITY OF THE TWO
C       DIMENSIONAL IMAGE OF A PLANE WAVE THROUGH A
C       THIN LENS AT SOME ANGLE ALPHA
C
C
      INTEGER IA1,IA2,N1,N2,N3,IJOB,IWK(2000),N
      INTEGER IARG,JARG,CENTER
      REAL RWK(2000),INT(256,256),X,Y,M(256,256),R1,R2
      REAL INDEX,PI,RAD,D,ARG2,F,ALPHA,MAX,ASTOP
      COMPLEX CWK(256),A(256,256),B(256,256)
C
      OPEN(UNIT=23,STATUS='NEW',FILE='APER.DAT')
      OPEN(UNIT=24,STATUS='NEW',FILE='DBGFFT.DAT')
      OPEN(UNIT=25,STATUS='NEW',FILE='TEST.DAT')
      OPEN(UNIT=26,STATUS='NEW',FILE='PERFECTA.DAT')
C
C     READ PARAMETERS
C
      N=256
      PI=3.1415927
      WRITE(5,29)
      READ(5,30) R1
      READ(5,30) R2
      READ(5,30) ASTOP
      READ(5,30) INDEX
      READ(5,30) ALPHA
      READ(5,31) CENTER
29    FORMAT(2X,'TYPE IN VALUES FOR R1,R2,ASTOP,INDEX,ALPHA, AND
* CENTER(0 OR 1), RETURN AFTER EACH ENTRY, REMEMBER PERIODS!')
30    FORMAT(F15.4)
31    FORMAT(I3)
      WRITE(5,30) R1
C
C     R1=RADIUS OF CURVATURE OF LEFT HAND SURFACE
C     R2=RADIUS OF CURVATURE OF RIGHT HAND SURFACE
C     ASTOP=RADIUS OF APERTURE STOP OF THE SYSTEM
C     INDEX=INDEX OF REFRACTION OF THE LENS MEDIUM
C     F=FOCAL LENGTH OF THE THIN LENS
C     ALPHA=ANGLE OF INCIDENCE FOR PLANE WAVE
C     CENTER=WHETHER OR NOT YOU WANT THE INTENSITY GRAPHED
C         CENTERED ON THE MAXIMUM OR NOT
C
```

```
      ALPHA=ALPHA*PI/180.
      F=1./((INDEX-1.)*(1/R1-1/R2))
      DELX=ASTOP/17.
C
C     CREATE APERTURE
C
      DO 220 I=1,N
       XI=I
       DO 200 J=1,N
        YJ=J
        RAD=DELX*SQRT((XI-(127.+0.5))**2+(YJ-(127.+0.5))**2)
        X=(XI-(127.+0.5))*DELX
        Y=(YJ-(127.+0.5))*DELX
        IF(RAD.LT.ASTOP) GO TO 60
        IF(RAD.GT.ASTOP) GO TO 100
60        D=-R1*(1.-SQRT(1.-((X**2+Y**2)/R1**2)))+
     @          R2*(1.-SQRT(1.-((X**2+Y**2)/R2**2)))
          ARG1=PI*(X**2+Y**2)/F
          ARG2=2.*PI*(INDEX-1.)*D+ARG1-2.*PI*X*SIN(ALPHA)
          IF(I.EQ.128) THEN
           WRITE(24,87) J,X,Y,D,ARG1,ARG2
87          FORMAT(2X,I3,5(3X,1PE11.4))
          ENDIF
          A(I,J)=CMPLX(COS(ARG2),SIN(ARG2))
          GO TO 120
100       A(I,J)=(0.0,0.0)
120       CONTINUE
200     CONTINUE
220   CONTINUE
C
C     OUTPUT APERTURE MATRIX
C
      DO 230 I=90,127
       DO 225 J=90,127
         WRITE(23,40) I,J,A(I,J)
40        FORMAT(2X,I3,3X,I3,2(3X,1PE11.4))
225    CONTINUE
230   CONTINUE
C
C
C     PERFORM FAST FOURIER TRANSFORM USING IMSL
C
C
240   IA1=N
      IA2=N
      N1=N
      N2=N
```

```
      N3=1
      IJOB=1
      CALL FFT3D (A,IA1,IA2,N1,N2,N3,IJOB,IWK,RWK,CWK)
C
C     OUTPUT NEW MATRIX A
C
      DO 242 J=1,N
        I=127
        WRITE(24,40) I,J,A(I,J)
40       FORMAT(2X,I3,3X,I3,2(3X,1PE11.4))
242     CONTINUE
C
C
      IF(CENTER.EQ.1) GO TO 767
      IF(CENTER.EQ.0) THEN
C
C     SHIFT ZERO FREQUENCY TO ARRAY CENTER
C
C
      DO 260 I=1,256
        DO 255 J=1,128
          B(I,J)=A(I,J+128)
          B(I,J+128)=A(I,J)
255       CONTINUE
260     CONTINUE
      DO 270 J=1,256
        DO 265 I=1,128
          A(I,J)=B(I+128,J)
          A(I+128,J)=B(I,J)
265       CONTINUE
270     CONTINUE
C
C
C     REDUCE SIZE OF ARRAY
C
C
      DO 250 I=1,96
        DO 245 J=1,96
          B(I,J)=A(I+80,J+80)
245       CONTINUE
250     CONTINUE
C
C
C     WRITE CENTERED A MATRIX
C
      DO 274 I=1,96
        DO 272 J=1,96
```

```
      WRITE(25,40) I,J,B(I,J)
272     CONTINUE
274   CONTINUE
C
C
C     CALCULATE THE MODULUS AND INTENSITY OF ARRAY
C
C
      DO 400 I=1,96
        DO 380 J=1,96
          M(I,J)=CABS(B(I,J))
          INT(I,J)=M(I,J)**2
380     CONTINUE
400   CONTINUE
C
C
C     FIND THE POINT OF MAXIMUM INTENSITY
C
      MAX=0.0
      DO 343 I=1,96
        DO 342 J=1,96
          IF(INT(I,J).GT.MAX) THEN
            IMAX=I
            JMAX=J
            MAX=INT(I,J)
          ENDIF
342     CONTINUE
343   CONTINUE
C
C
C     OUTPUT OF INTENSITY
C
      IMAX=IMAX+80
      JMAX=JMAX+80
      WRITE(26,134) IMAX,JMAX,MAX
134   FORMAT(2X,I3,3X,I3,3X,1PE11.4)
      DO 404 I=1,96
        DO 402 J=1,96
          WRITE(26,41) I,J,INT(I,J)
41      FORMAT(2X,I3,3X,I3,3X,1PE11.4)
402     CONTINUE
404   CONTINUE
C
C
      ENDIF
      GO TO 999
C ***************************************************************************
```

```
C
C     TO GRAPH MAXIMUM INTENSITY AT CENTER OF PLOT
C
C     SHIFT ZERO FREQUENCY TO ARRAY CENTER
C
767    DO 654 I=1,256
       DO 653 J=1,128
         B(I,J)=A(I,J+128)
         B(I,J+128)=A(I,J)
653      CONTINUE
654    CONTINUE
      DO 652 J=1,256
       DO 651 I=1,128
         A(I,J)=B(I+128,J)
         A(I+128,J)=B(I,J)
651      CONTINUE
652    CONTINUE
C
C
C     CALCULATE THE MODULUS AND INTENSITY OF THE ARRAY
C
C
      DO 721 I=1,256
       DO 720 J=1,256
         M(I,J)=CABS(A(I,J))
         INT(I,J)=M(I,J)**2
720      CONTINUE
721    CONTINUE
C
C
C     FIND THE POINT OF MAXIMUM INTENSITY
C
      MAX=0.0
      DO 124 I=1,256
       DO 123 J=1,256
         IF(INT(I,J).GT.MAX) THEN
           IMAX=I
           JMAX=J
           MAX=INT(I,J)
         ENDIF
123      CONTINUE
124    CONTINUE
C
C
C     SELECT BOX TO GRAPH
C
      IOFFSET=IMAX-48-1
```

```
      JOFFSET=JMAX-48-1
C
      IF(IOFFSET.LT.1) THEN
        IOFFSET=0
      ENDIF
      IF(IOFFSET+96.GT.256) THEN
        IOFFSET=256-96-1
      ENDIF
C
      IF(JOFFSET.LT.1) THEN
        JOFFSET=0
      ENDIF
      IF(JOFFSET+96.GT.256) THEN
        JOFFSET=256-96-1
      ENDIF
C
      DO 542 I=1,96
        DO 541 J=1,96
          M(I,J)=INT(IOFFSET+I,JOFFSET+J)
541     CONTINUE
542   CONTINUE
C
C
C     OUTPUT OF INTENSITY
C
      WRITE(26,34) IMAX,JMAX,MAX
34    FORMAT(2X,I3,3X,I3,3X,1PE11.4)
      DO 702 I=1,96
        DO 701 J=1,96
          WRITE(26,73) I,J,M(I,J)
73        FORMAT(2X,I3,3X,I3,3X,1PE11.4)
701     CONTINUE
702   CONTINUE
999   STOP
      END
```

APPENDIX B

This appendix contains the code for the program ALPHA. This program calculates the far-field intensity pattern of the impulse response for the Walton thin lens at various angles of incident radiation (with respect to the optic axis). The aperture is defined by the knowns: the two radii of curvature for the lens, the height and aperture stop for the lens, and the angle of incidence α. The various distances through the lens are then calculated for various x and y coordinates in the central plane of the lens as is defined in Figure 11. These distances are then computed as phase lags for the incident plane wave (at an arbitrary angle). This aperture is then Fresnel propagated to the image plane where the intensity plots are computed, and given in the text. The parameters, as well as other dimensions determined by the computer, are in the units of pixels. The optic axis is centered on the position (128.5,128.5) in the object plane, and in the image plane the system rounds the optic axis to be at the position (129,129).

```
C     PROGRAM:  ALPHA.F
C       THIS PROGRAM CALCULATES THE INTENSITY OF THE TWO
C       DIMENSIONAL IMAGE OF A PLANE WAVE THROUGH A
C       THIN LENS AT SOME ANGLE ALPHA
C
C
      INTEGER IA1,IA2,N1,N2,N3,IJOB,IWK(2000),N
      INTEGER F1,F2,CENTER
      REAL RWK(2000),INT(256,256),X,Y,M(256,256),R1,R2,H,ALPHA
      REAL INDEX,PI,RAD,BETA,ETA,XSIM,XSIP,ARG1,ARG2,F,MAX
      REAL LAMBDA,D(256,256),ARG3,ARG4
      COMPLEX CWK(256),A(256,256),B(256,256)
C
      OPEN(UNIT=23,STATUS='NEW',FILE='SURFACE.DAT')
      OPEN(UNIT=24,STATUS='NEW',FILE='DBGFFT.DAT')
      OPEN(UNIT=25,STATUS='NEW',FILE='ALPHA.DAT')
      OPEN(UNIT=26,STATUS='NEW',FILE='ALPHA.DAT')
      OPEN(UNIT=27,STATUS='NEW',FILE='MILLSA.DAT')
C
C     READ PARAMETERS
C
      N=256
      PI=3.1415927
      WRITE(5,29)
      READ(5,30) R1
      READ(5,30) R2
      READ(5,30) H
      READ(5,30) ASTOP
      READ(5,30) ALPHA
      READ(5,30) INDEX
      READ(5,31) CENTER
29    FORMAT(2X,'TYPE IN VALUES FOR R1,R2,H,ASTOP,ALPHA,INDEX
     * AND CENTER, RETURN AFTER EACH ENTRY, REMEMBER PERIODS!')
31    FORMAT(I3)
30    FORMAT(F15.4)
C
C     R1=RADIUS OF CURVATURE OF LEFT HAND SURFACE
C     R2=RADIUS OF CURVATURE OF RIGHT HAND SURFACT
C     H=HEIGHT OF LENS FROM OPTIC AXIS AT CENTER OF LENS
C     ALPHA=ANGLE WITH RESPECT TO OPTIC AXIS OF INCIDENT
C         PLANE WAVE
C     INDEX=INDEX OF REFRACTION OF THE LENS MEDIUM
C     F=FOCAL LENGTH OF THE THIN LENS
C     LAMBDA=WAVELENGTH USED IN EXPERIMENT (HENE = .6328E-6)
C
      ALPHA=ALPHA*PI/180.
      F=1./((INDEX-1.)*(1/R1-1/R2))
```

```
      DELX=ASTOP/17.
      LAMBDA=.6328
      WRITE(5,30) ALPHA
C
C     CREATE APERTURE
C
      DO 220 I=1,N
       XI=I
       DO 200 J=1,N
        YJ=J
        RAD=DELX*SQRT((XI-(127.+0.5))**2.+(YJ-(127.+0.5))**2.)
        X=(XI-(127.+0.5))*DELX
        Y=(YJ-(127.+0.5))*DELX
        IF(RAD.LT.ASTOP) GO TO 60
        IF(RAD.GT.ASTOP) GO TO 100
60        BETA=1./(COS(ALPHA)**2.)
          ETA=X**2.+Y**2.-H**2.
          XSIM=(SQRT(R2**2.-H**2.))-Y*TAN(ALPHA)
          XSIP=(SQRT(R1**2.-H**2.))+Y*TAN(ALPHA)
          D(I,J)=COS(ALPHA)*((SQRT(XSIM**2.-ETA*BETA))+
     *       (SQRT(XSIP**2.-ETA*BETA))-XSIM-XSIP)
          ARG1=PI*(X**2.+Y**2.)*10**4/(F*LAMBDA)
          ARG2=2.*PI*Y*SIN(ALPHA)*10**4/LAMBDA
          ARG3=2.*PI*(INDEX-1.)*D(I,J)*10**4/LAMBDA
          ARG4=ARG3+ARG1-ARG2
          WRITE(27,97) I,J,D(I,J),ARG1,ARG2,ARG3,ARG4
97         FORMAT(2X,2(I3,3X),5(1PE11.4,3X))
          IF(I.EQ.127) THEN
           WRITE(27,98) J,RAD,X,Y,BETA,ETA,XSIM,XSIP
           WRITE(27,99) D,ARG1,ARG2
98          FORMAT(2X,I3,7(2X,1PE11.4))
99          FORMAT(15X,3(1PE11.4,2X))
          ENDIF
          A(I,J)=CMPLX(COS(ARG4),SIN(ARG4))
          GO TO 120
100       A(I,J)=(0.0,0.0)
          D(I,J)=0.0
120       CONTINUE
200     CONTINUE
220   CONTINUE
C
C     OUTPUT APERTURE MATRIX
C
      DO 230 I=104,151
       DO 225 J=104,151
        IF(REAL(A(I,J)).EQ.0.) THEN
         M(I,J)=0.0
```

```
          ELSE
            M(I,J)=ATAN(AIMAG(A(I,J))/REAL(A(I,J)))
          ENDIF
225       CONTINUE
230     CONTINUE
C
C
C       PERFORM FAST FOURIER TRANSFORM USING IMSL
C
C
240     LA1=N
        LA2=N
        N1=N
        N2=N
        N3=1
        IJOB=1
        CALL FFT3D (A,LA1,LA2,N1,N2,N3,IJOB,IWK,RWK,CWK)
C
C       OUTPUT NEW MATRIX A
C
        DO 242 J=1,N
          I=127
          WRITE(24,40) I,J,A(I,J)
40        FORMAT(2X,I3,3X,I3,2(3X,1PE11.4))
242     CONTINUE
C
C
        IF(CENTER.EQ.1) GO TO 767
        IF(CENTER.EQ.0) THEN
C
C
C       SHIFT ZERO FREQUENCY TO ARRAY CENTER
C
C
        DO 260 I=1,256
          DO 255 J=1,128
            B(I,J)=A(I,J+128)
            B(I,J+128)=A(I,J)
255       CONTINUE
260     CONTINUE
        DO 270 J=1,256
          DO 265 I=1,128
            A(I,J)=B(I+128,J)
            A(I+128,J)=B(I,J)
265       CONTINUE
270     CONTINUE
C
```

```
C
C     REDUCE SIZE OF ARRAY
C
C
      DO 250 I=1,96
       DO 245 J=1,96
        B(I,J)=A(I+80,J+80)
245     CONTINUE
250    CONTINUE
C
C
C     WRITE CENTERED A MATRIX
C
      DO 274 I=1,96
       DO 272 J=1,96
       WRITE(25,40) I,J,B(I,J)
272     CONTINUE
274    CONTINUE
C
C
C     CALCULATE THE MODULUS AND INTENSITY OF ARRAY
C
C
      DO 400 I=1,96
       DO 380 J=1,96
        M(I,J)=CABS(B(I,J))
        INT(I,J)=M(I,J)**2
380     CONTINUE
400    CONTINUE
C
C
C     FIND THE POINT OF MAXIMUM INTENSITY
C
      MAX=0.0
      DO 343 I=1,96
       DO 342 J=1,96
        IF(INT(I,J).GT.MAX) THEN
         IMAX=I
         JMAX=J
         MAX=INT(I,J)
        ENDIF
342     CONTINUE
343    CONTINUE
C
C
C     OUTPUT OF INTENSITY
C
```

```
721   CONTINUE
C
      DO 368 J=1,256,2
       WRITE(24,23) J,INT(129,J),J+1,INT(129,J+1)
23     FORMAT(2X,2(I3,3X,1PE11.4,3X))
368   CONTINUE
C
C     FIND THE POINT OF MAXIMUM INTENSITY
C
      MAX=0.0
      DO 124 I=1,256
       DO 123 J=1,256
        IF(INT(I,J).GT.MAX) THEN
         IMAX=I
         JMAX=J
         MAX=INT(I,J)
        ENDIF
123     CONTINUE
124   CONTINUE
C
C
C     SELECT BOX TO GRAPH
C
      IOFFSET=IMAX-48-1
      JOFFSET=JMAX-48-1
C
      IF(IOFFSET.LT.1) THEN
       IOFFSET=0
      ENDIF
      IF(IOFFSET+96.GT.256) THEN
       IOFFSET=256-96-1
      ENDIF
C
      IF(JOFFSET.LT.1) THEN
       JOFFSET=0
      ENDIF
      IF(JOFFSET+96.GT.256) THEN
       JOFFSET=256-96-1
      ENDIF
C
      CMAX=0.0
      DO 542 I=1,96
       DO 541 J=1,96
        M(I,J)=INT(IOFFSET+I,JOFFSET+J)
        IF(M(I,J).GT.CMAX) THEN
         MAXI=I
         MAXJ=J
```

```
            CMAX=M(I,J)
          ENDIF
541       CONTINUE
542     CONTINUE
C
C
C       OUTPUT OF INTENSITY
C
        WRITE(26,73) IMAX,JMAX,MAX
73      FORMAT(2X,I3,3X,I3,3X,1PE11.4)
        DO 702 I=1,96
          DO 701 J=1,96
            WRITE(26,73) I,J,M(I,J)
701       CONTINUE
702     CONTINUE
999     STOP
        END
```

APPENDIX C

This appendix contains the code for the program ZERNIKE. This program calculates the far-field intensity pattern of the impulse response for the two lenses at various angles of incident radiation. The aberration coefficients were first calculated by the ray trace program FALCON, and then these coefficients were mapped onto a unit circle which is the exit pupil of the optical system. These values were then entered into a Fast Fourier Transform, and the intensity plots were calculated by squaring the output of the transform. The optic axis is centered on the position (128.5,128.5) in the object plane, and in the image plane the system rounds the optic axis to be at the position (129,129).

```
C
C       PROGRAM:  MZERNIKE.F
C
C
C       THIS PROGRAM CALCULATES THE INTENSITY OF THE TWO
C       DIMENSIONAL IMAGE OF A PLANE WAVE THROUGH A
C       LENS WITH THE APPROPRIATE ZERNIKE ABERRATIONS AT SOME
C       ANGLE ALPHA
C
C
      INTEGER IA1,IA2,N1,N2,N3,IJOB,IWK(2000),N
      INTEGER IARG,JARG,CENTER
      REAL RWK(2000),INT(256,256),X,Y,M(256,256),R1,R2
      REAL INDEX,PI,RAD,ARG2,FOCAL,MAX,H,LAMBDA
      COMPLEX CWK(256),A(256,256),B(256,256)
C
      OPEN(UNIT=23,STATUS='NEW',FILE='APER.DAT')
      OPEN(UNIT=24,STATUS='NEW',FILE='DBGFFT.DAT')
      OPEN(UNIT=25,STATUS='NEW',FILE='TEST.DAT')
      OPEN(UNIT=26,STATUS='NEW',FILE='ZERNIKE.DAT')
C
C     READ PARAMETERS
C
      N=256
      LAMBDA=.6328
      PI=3.1415927
      WRITE(5,29)
      READ(5,30) R1
      READ(5,30) R2
      READ(5,30) ALPHA
      READ(5,30) INDEX
      READ(5,30) A1
      READ(5,30) A2
      READ(5,30) A3
      READ(5,30) A4
      READ(5,30) A5
      READ(5,30) A6
      READ(5,30) A7
      READ(5,30) A8
      READ(5,31) CENTER
29     FORMAT(2X,'TYPE IN VALUES FOR R1,R2,ALPHA,INDEX,A1-8, AND
     * CENTER(0 OR 1) RETURN AFTER EACH ENTRY, REMEMBER PERIODS!')
30     FORMAT(F15.4)
31     FORMAT(I3)
      WRITE(5,30) R1
C
C     R1=RADIUS OF CURVATURE OF LEFT HAND SURFACE
```

```
C     R2=RADIUS OF CURVATURE OF RIGHT HAND SURFACE
C     INDEX=INDEX OF REFRACTION OF THE LENS MEDIUM
C     FOCAL=FOCAL LENGTH OF THE THIN LENS
C     A1-8=THE ZERNIKE COEFFICIENTS : TILT,FOCUS,ASTIGMATISM,COMA,
C        AND SPHERICAL
C     CENTER=WHETHER OR NOT YOU WANT THE INTENSITY GRAPH TO
C        CENTERED ON THE MAXIMUM OR NOT
C
      FOCAL=1./((INDEX-1.)*(1/R1-1/R2))
      ALPHA=ALPHA*PI/180.
C
C     CREATE APERTURE
C
      DO 220 I=1,N
       XI=I
       DO 200 J=1,N
        YJ=J
        RAD=SQRT((XI-(127.+0.5))**2+(YJ-(127.+0.5))**2)/17.
        X=(XI-(127.+0.5))/17.
        Y=(YJ-(127.+0.5))/17.
        IF(RAD.LT.1.) GO TO 60
        IF(RAD.GT.1.) GO TO 100
60        PHI = A1*Y + A2*X + A3*(-1.+2.*Y**2+2.*X**2)
     *        + A5*2.*X*Y + A4*(Y**2-X**2)
     *        + A6*(-2.*Y+3.*Y**3+3.*Y*X**2)
     *        + A7*(-2.*X+3.*X*Y**2+3.*X**3)
     *        + A8*(1.-6.*Y**2-6.*X**2+6.*Y**4+
     *             12.*X**2*Y**2+6.*X**4)
          ARG2=2.*PI*PHI - 2.*PI*Y*SIN(ALPHA)*10**4/LAMBDA
          A(I,J)=CMPLX(COS(ARG2),SIN(ARG2))
          GO TO 120
100       A(I,J)=(0.0,0.0)
120       CONTINUE
200     CONTINUE
220   CONTINUE
C
C     OUTPUT APERTURE MATRIX
C
      DO 230 I=90,127
       DO 225 J=90,127
         WRITE(23,40) I,J,A(I,J)
40        FORMAT(2X,I3,3X,I3,2(3X,1PE11.4
225     CONTINUE
230   CONTINUE
C
C
C     PERFORM FAST FOURIER
```

```
C
C
240   IA1=N
      IA2=N
      N1=N
      N2=N
      N3=1
      IJOB=1
      CALL FFT3D (A,IA1,IA2,N1,N2,N3,IJOB,IWK,RWK,CWK)
C
C     OUTPUT NEW MATRIX A
C
      DO 242 J=1,N
        I=127
        WRITE(24,40) I,J,A(I,J)
40      FORMAT(2X,I3,3X,I3,2(3X,1PE11.4))
242   CONTINUE
C
C
      IF(CENTER.EQ.1) GO TO 767
      IF(CENTER.EQ.0) THEN
C
C     SHIFT ZERO FREQUENCY TO ARRAY CENTER
C
C
      DO 260 I=1,256
        DO 255 J=1,128
          B(I,J)=A(I,J+128)
          B(I,J+128)=A(I,J)
255     CONTINUE
260   CONTINUE
      DO 270 J=1,256
        DO 265 I=1,128
          A(I,J)=B(I+128,J)
          A(I+128,J)=B(I,J)
265     CONTINUE
270   CONTINUE
C
C
C     REDUCE SIZE OF ARRAY
C
C
      DO 250 I=1,96
        DO 245 J=1,96
          B(I,J)=A(I+80,J+80)
245     CONTINUE
250   CONTINUE
```

```
C
C
C     WRITE CENTERED A MATRIX
C
      DO 274 I=1,96
       DO 272 J=1,96
       WRITE(25,40) I,J,B(I,J)
272     CONTINUE
274    CONTINUE
C
C
C     CALCULATE THE MODULUS AND INTENSITY OF ARRAY
C
C
      DO 400 I=1,96
       DO 380 J=1,96
         M(I,J)=CABS(B(I,J))
         INT(I,J)=M(I,J)**2
380     CONTINUE
400    CONTINUE
C
C
C     FIND THE POINT OF MAXIMUM INTENSITY
C
      MAX=0.0
      DO 343 I=1,96
       DO 342 J=1,96
         IF(INT(I,J).GT.MAX) THEN
           IMAX=I
           JMAX=J
           MAX=INT(I,J)
         ENDIF
342     CONTINUE
343    CONTINUE
C
C
C     OUTPUT OF INTENSITY
C
      IMAX=IMAX+80
      JMAX=JMAX+80
      WRITE(26,134) IMAX,JMAX,MAX
134    FORMAT(2X,I3,3X,I3,3X,1PE11.4)
      DO 404 I=1,96
       DO 402 J=1,96
         WRITE(26,41) I,J,INT(I,J)
41      FORMAT(2X,I3,3X,I3,3X,1PE11.4)
402     CONTINUE
```

```
404   CONTINUE
C
C
      ENDIF
      GO TO 999
C  ***********************************************************************
C
C     TO GRAPH MAXIMUM INTENSITY AT CENTER OF PLOT
C
C     SHIFT ZERO FREQUENCY TO ARRAY CENTER
C
767   DO 654 I=1,256
       DO 653 J=1,128
        B(I,J)=A(I,J+128)
        B(I,J+128)=A(I,J)
653     CONTINUE
654   CONTINUE
      DO 652 J=1,256
       DO 651 I=1,128
        A(I,J)=B(I+128,J)
        A(I+128,J)=B(I,J)
651     CONTINUE
652   CONTINUE
C
C
C     CALCULATE THE MODULUS AND INTENSITY OF THE ARRAY
C
C
      DO 721 I=1,256
       DO 720 J=1,256
        M(I,J)=CABS(A(I,J))
        INT(I,J)=M(I,J)**2
720     CONTINUE
721   CONTINUE
C
C
C     FIND THE POINT OF MAXIMUM INTENSITY
C
      MAX=0.0
      DO 124 I=1,256
       DO 123 J=1,256
        IF(INT(I,J).GT.MAX) THEN
         IMAX=I
         JMAX=J
         MAX=INT(I,J)
        ENDIF
123     CONTINUE
```

```
124   CONTINUE
C
C
C     SELECT BOX TO GRAPH
C
      IOFFSET=IMAX-48-1
      JOFFSET=JMAX-48-1
C
      IF(IOFFSET.LT.1) THEN
       IOFFSET=0
      ENDIF
      IF(IOFFSET+96.GT.256) THEN
       IOFFSET=256-96-1
      ENDIF
C
      IF(JOFFSET.LT.1) THEN
       JOFFSET=0
      ENDIF
      IF(JOFFSET+96.GT.256) THEN
       JOFFSET=256-96-1
      ENDIF
C
      CMAX=0.0
      DO 542 I=1,96
       DO 541 J=1,96
        M(I,J)=INT(IOFFSET+I,JOFFSET+J)
        IF(M(I,J).GT.CMAX) THEN
         MAXI=I
         MAXJ=J
         CMAX=M(I,J)
        ENDIF
541     CONTINUE
542   CONTINUE
C
C
C     OUTPUT OF INTENSITY
C
      WRITE(26,34) IMAX,JMAX,MAX
34    FORMAT(2X,I3,3X,I3,3X,1PE11.4)
      DO 702 I=1,96
       DO 701 J=1,96
        WRITE(26,73) I,J,M(I,J)
73       FORMAT(2X,I3,3X,I3,3X,1PE11.4)
701     CONTINUE
702   CONTINUE
999   STOP
      END
```

APPENDIX D

This appendix contains a representative code for multi-aperture systems. The program given is MULTI. This program computes the multi-aperture impulse response for the Walton thin lens at various angles α for various numbers of apertures at various placements in the field. Each lens or aperture is assumed to be exactly like any other aperture in the system. The aperture knowns are the same as in the program ALPHA. After the program has calculated the appropriate distances and therefore phase lags for one aperture, it then translates this aperture to various determined positions in the exit plane of the optical system. After the multi-aperture system is set up in the object plane, the field is then Fresnel propagated to the image plane where the intensity plots are computed, and given in the text. The parameters, as well as other dimensions determined by the computer, are in units of pixels. The optic axis is centered on the position (128.5,128.5) in the object plane, and in the image plane the system rounds the optic axis to be at the position (129,129).

```
C
C
C     PROGRAM:  MULTI.F
C
C
C       THIS PROGRAM CALCULATES THE INTENSITY OF THE TWO
C       DIMENSIONAL IMAGE OF A PLANE WAVE THROUGH A
C       MULTI APERTURE SYSTEM USING THE WALTON THIN
C       LENS AT SOME ANGLE ALPHA
C
C
      INTEGER IA1,IA2,N1,N2,N3,IJOB,IWK(2000),N
      INTEGER IARG,JARG,F1,F2,APE,CENTER
      REAL RWK(2000),INT(256,256),X,Y,M(256,256),R1,R2,H,ALPHA
      REAL INDEX,PI,RAD,BETA,ETA,XSIM,XSIP,D,ARG1,ARG2,F,ROT
      REAL LAMBDA,ASTOP,MAX,ARG3
      COMPLEX CWK(256),A(256,256),B(256,256)
C
      OPEN(UNIT=23,STATUS='NEW',FILE='APER.DAT')
      OPEN(UNIT=24,STATUS='NEW',FILE='DBGFFT.DAT')
      OPEN(UNIT=25,STATUS='NEW',FILE='MULTI.DAT')
      OPEN(UNIT=26,STATUS='NEW',FILE='MULTI.DAT')
      OPEN(UNIT=27,STATUS='NEW',FILE='MILLS1.DAT')
C
C     READ PARAMETERS
C
      N=256
      PI=3.1415927
      WRITE(5,29)
      READ(5,30) R1
      READ(5,30) R2
      READ(5,30) H
      READ(5,30) ASTOP
      READ(5,30) RADIUS
      READ(5,30) APER
      READ(5,30) ROT
      READ(5,30) ALPHA
      READ(5,30) INDEX
      READ(5,31) CENTER
   29   FORMAT(2X,'TYPE IN VALUES FOR R1,R2,H,ASTOP,RADIUS,APER,ROT
     * INDEX,AND CENTER, RETURN AFTER EACH ENTRY, REMEMBER PERIODS!')
   30   FORMAT(F15.4)
   31   FORMAT(I3)
C
C     R1=RADIUS OF CURVATURE OF LEFT HAND SURFACE
C     R2=RADIUS OF CURVATURE OF RIGHT HAND SURFACE
C     H=HEIGHT OF LENS FROM OPTIC AXIS AT CENTER OF LENS
```

```
C     ASTOP=RADIUS OF THE APERTURE STOP OF THE SYSTEM
C     RADIUS=OUTER RADIUS OF SYNTHESIZED APERTURE
C          (EXPRESSED AS MULTIPLE OF SUB-APERTURE RADIUS)
C     APER=NUMBER OF SUB-APERTURES IN THE ARRAY
C     ROT=ROTATION OF ARRAY (DEGREES)
C     ALPHA=ANGLE WITH RESPECT TO OPTIC AXIS OF INCIDENT
C          PLANE WAVE
C     INDEX=INDEX OF REFRACTION OF THE LENS MEDIUM
C     LAMBDA=WAVELENGTH OF INTEREST
C     F=FOCAL LENGTH OF THE THIN LENS
C
      ALPHA=ALPHA*PI/180.
      DELX=ASTOP/17.
      LAMBDA=.6328
      ROT=ROT*PI/180.
      F=1./((INDEX-1.)*(1/R1-1/R2))
      SDIAM=2.*17.
      APE=APER-1.
      ORAD=RADIUS*17.
      WRITE(5,30) ALPHA
C
C     CREATE APERTURE
C
C
C      FIRST APERTURE
C
      IARG=128-17.+(ORAD-17.)*COS(ROT)
      JARG=128-17.+(ORAD-17.)*SIN(ROT)
C
      DO 107 I=1,N
       DO 105 J=1,N
        A(I,J)=CMPLX(0,0)
105    CONTINUE
107   CONTINUE
C
      DO 220 I=1,SDIAM
       XI=I
       DO 200 J=1,SDIAM
        YJ=J
        RAD=DELX*SQRT((XI-(17.+1.5))**2.+(YJ-(17.+1.5))**2.)
        X=(XI-(17.+1.5))*DELX
        Y=(YJ-(17.+1.5))*DELX
        IF(RAD.LT.ASTOP) GO TO 60
        IF(RAD.GT.ASTOP) GO TO 100
60        BETA=1./(COS(ALPHA)**2.)
          ETA=X**2.+Y**2.-H**2.
          XSIM=(SQRT(R2**2.-H**2.))-Y*TAN(ALPHA)
```

```
          XSIP=(SQRT(R1**2.-H**2.))+Y*TAN(ALPHA)
          D=COS(ALPHA)*((SQRT(XSIM**2.-ETA*BETA))+
     *       (SQRT(XSIP**2.-ETA*BETA))-XSIM-XSIP)
          ARG1=PI*(X**2.+Y**2.)/F
          ARG2=2.*PI*(INDEX-1.)*D+ARG1-2.*PI*X*SIN(ALPHA)
          ARG3=ARG2*10**4/LAMBDA
          IF(I.EQ.127) THEN
            WRITE(27,98) J,BETA,ETA,XSIM,XSIP,D,ARG1,ARG2
98          FORMAT(2X,I3,7(3X,1PE11.4))
          ENDIF
          A(I+IARG,J+JARG)=CMPLX(COS(ARG3),SIN(ARG3))
          GO TO 120
100       A(I+IARG,J+JARG)=(0.0,0.0)
120       CONTINUE
200     CONTINUE
220   CONTINUE
C
C
C       CREATE REMAINING SUB-APERTURES
C
C
      DO 227 I=1,APE
       U=(ORAD-17.)*COS(I*2.*PI/APER+ROT)
       V=(ORAD-17.)*SIN(I*2.*PI/APER+ROT)
       XP=127.-17.+U
       YP=127.-17.+V
       DO 225 J=1,SDIAM
         DO 223 K=1,SDIAM
           A(XP+J,YP+K)=A(XP+J,YP+K)+A(J+IARG,K+JARG)
223        CONTINUE
225      CONTINUE
227    CONTINUE
C
C
C      OUTPUT APERTURE MATRIX
C
      DO 230 I=110,127
       DO 229 J=110,127
         WRITE(23,40) I,J,A(I,J)
40        FORMAT(2X,I3,3X,I3,2(3X,1PE11.4))
229      CONTINUE
230    CONTINUE
C
C
C      PERFORM FAST FOURIER TRANSFORM USING IMSL
C
C
```

```
240   IA1=N
      IA2=N
      N1=N
      N2=N
      N3=1
      IJOB=1
      CALL FFT3D (A,IA1,IA2,N1,N2,N3,IJOB,IWK,RWK,CWK)
C
C     OUTPUT NEW MATRIX A
C
      DO 242 J=1,N
       I=127
       WRITE(24,40) I,J,A(I,J)
40      FORMAT(2X,I3,3X,I3,2(3X,1PE11.4))
242   CONTINUE
C
C
      IF(CENTER.EQ.1) GO TO 767
      IF(CENTER.EQ.0) THEN
C
C
C     SHIFT ZERO FREQUENCY TO ARRAY CENTER
C
C
      DO 260 I=1,256
       DO 255 J=1,128
        B(I,J)=A(I,J+128)
        B(I,J+128)=A(I,J)
255     CONTINUE
260   CONTINUE
      DO 270 J=1,256
       DO 265 I=1,128
        A(I,J)=B(I+128,J)
        A(I+128,J)=B(I,J)
265     CONTINUE
270   CONTINUE
C
C
C     REDUCE SIZE OF ARRAY
C
C
      DO 250 I=1,96
       DO 245 J=1,96
        B(I,J)=A(I+80,J+80)
245     CONTINUE
250   CONTINUE
C
```

```
C
C     WRITE CENTERED A MATRIX
C
      DO 274 I=1,96
       DO 272 J=1,96
       WRITE(25,40) I,J,B(I,J)
272     CONTINUE
274    CONTINUE
C
C
C     CALCULATE THE MODULUS AND INTENSITY OF ARRAY
C
C
      DO 400 I=1,96
       DO 380 J=1,96
         M(I,J)=CABS(B(I,J))
         INT(I,J)=M(I,J)**2
380     CONTINUE
400    CONTINUE
C
C
C     FIND THE POINT OF MAXIMUM INTENSITY
C
      MAX=0.0
      DO 343 I=1,96
       DO 342 J=1,96
         IF(INT(I,J).GT.MAX) THEN
           IMAX=I
           JMAX=J
           MAX=INT(I,J)
         ENDIF
342     CONTINUE
343    CONTINUE
C
C
C     OUTPUT OF INTENSITY
C
      IMAX=IMAX+80
      JMAX=JMAX+80
      WRITE(26,134) IMAX,JMAX,MAX
134    FORMAT(2X,I3,3X,I3,3X,1PE11.4)
      DO 404 I=1,96
       DO 402 J=1,96
         WRITE(26,41) I,J,INT(I,J)
41      FORMAT(2X,I3,3X,I3,3X,1PE11.4)
402     CONTINUE
404    CONTINUE
```

```
C
      END IF
      GO TO 999
C
C     ****************************************************************
C
C      TO GRAPH MAXIMUM INTENSITY AT CENTER OF PLOT
C
C      SHIFT ZERO FREQUENCY TO ARRAY CENTER
C
C
767    DO 654 I=1,256
       DO 653 J=1,128
         B(I,J)=A(I,J+128)
         B(I,J+128)=A(I,J)
653     CONTINUE
654    CONTINUE
      DO 652 J=1,256
       DO 651 I=1,128
         A(I,J)=B(I+128,J)
         A(I+128,J)=B(I,J)
651     CONTINUE
652    CONTINUE
C
C
C      CALCULATE THE MODULUS AND INTENSITY OF THE ARRAY
C
C
      DO 721 I=1,256
       DO 720 J=1,256
         M(I,J)=CABS(A(I,J))
         INT(I,J)=M(I,J)**2
720     CONTINUE
721    CONTINUE
C
C
C      FIND THE POINT OF MAXIMUM INTENSITY
C
      MAX=0.0
      DO 124 I=1,256
       DO 123 J=1,256
         IF(INT(I,J).GT.MAX) THEN
           IMAX=I
           JMAX=J
           MAX=INT(I,J)
         ENDIF
123     CONTINUE
```

```
124   CONTINUE
C
C
C     SELECT BOX TO GRAPH
C
      IOFFSET=IMAX-48-1
      JOFFSET=JMAX-48-1
C
      IF(IOFFSET.LT.1) THEN
        IOFFSET=0
      ENDIF
      IF(IOFFSET+96.GT.256) THEN
        IOFFSET=256-96-1
      ENDIF
C
      IF(JOFFSET.LT.1) THEN
        JOFFSET=0
      ENDIF
      IF(JOFFSET+96.GT.256) THEN
        JOFFSET=256-96-1
      ENDIF
C
      DO 542 I=1,96
        DO 541 J=1,96
          M(I,J)=INT(IOFFSET+I,JOFFSET+J)
541     CONTINUE
542   CONTINUE
C
C
C     OUTPUT OF INTENSITY
C
      WRITE(26,73) IMAX,JMAX,MAX
73    FORMAT(2X,I3,3X,I3,3X,1PE11.4)
      DO 702 I=1,96
        DO 701 J=1,96
          WRITE(26,73) I,J,M(I,J)
701     CONTINUE
702   CONTINUE
999   STOP
      END
```

Bibliography

1. Goodman, J.W. Introduction to Fourier Optics. San Francisco: McGraw-Hill Book Co., 1968.

2. Brookner, E. "Phased Array Radars," Scientific American, 252: 94-102 (February 1985).

3. Geary, J. and P. Peterson. "Spherical Aberration and Diffraction Derived via Fourier Optics," Optical Engineering, 23: 94-102 (February 1985)

4. Fender, Janet S. "Synthetic Apertures: An Overview," Proceedings of SPIE - The International Society for Optical Engineering, 440: 2-7 (August 1983).

5. Watson, Maj. Steven M. Two Point Resolution Criterion for Multi-Aperture Optical Systems. MS thesis, AFIT/GEP/ENP/87M-1. School of Engineering, Air Force Institute of Technology (AU). Wright-Patterson AFB OH. March 1987.

6. Bergey, Lt. Dana J. Coherent Multiple Aperture Optical Imaging Systems: Analysis and Design. MS thesis, AFIT/GE/ENG/87M-1. School of Engineering, Air Force Institute of Technology (AU), Wright-Patterson AFB OH, March 1987.

7. Fender, Janet S., Dr. Personal interview. Air Force Weapons Laboratory (AFSC), Kirtland AFB NM, March 1987.

8. Born M. and E. Wolf. Principles of Optics: Electromagnetic Theory of Propagation, Interference and Diffraction of Light. New York NY: MacMillan Co., 1964.

9. Airy, G. B. "On the diffraction of an object-glass with circular aperture." Trans. Camb. Phil. Soc. 5,283 (1835).

10. Mills, James P., LtCol USAF. Personal interview. Air Force Institute of Technology (AU), Wright-Patterson AFB OH, August 1987.

11. University of Dayton Research Institute. FALCON User's Manual. Report Number UDR-TR-81-16. Dayton OH, 1981.

12. Hecht E. and A. Zajac. Optics. Addison-Wesley Publishing Co., 1974.

VITA

Lieutenant Christina N. Walton was born [redacted] In 1982 she graduated [redacted] and attended the University of Southern California on an AFROTC scholarship. In 1986, she graduated and received the degree of Bachelor of Science in Electrical Engineering. Lieutenant Walton received a Reserve commission in the USAF and reported directly to the Air Force Institute of Technology.

Permanent Address: [redacted]

REPORT DOCUMENTATION PAGE

Form Approved
OMB No. 0704-0188

1a. REPORT SECURITY CLASSIFICATION UNCLASSIFIED	1b. RESTRICTIVE MARKINGS
2a. SECURITY CLASSIFICATION AUTHORITY	3. DISTRIBUTION/AVAILABILITY OF REPORT Approved for public release; distribution unlimited.
2b. DECLASSIFICATION/DOWNGRADING SCHEDULE	
4. PERFORMING ORGANIZATION REPORT NUMBER(S) AFIT/GEP/ENP/87D-10	5. MONITORING ORGANIZATION REPORT NUMBER(S)
6a. NAME OF PERFORMING ORGANIZATION School of Engineering 6b. OFFICE SYMBOL (If applicable) AFIT/ENP	7a. NAME OF MONITORING ORGANIZATION
6c. ADDRESS (City, State, and ZIP Code) Air Force Institute of Technology Wright-Patterson AFB, OH 45433-6583	7b. ADDRESS (City, State, and ZIP Code)
8a. NAME OF FUNDING/SPONSORING ORGANIZATION 8b. OFFICE SYMBOL (If applicable)	9. PROCUREMENT INSTRUMENT IDENTIFICATION NUMBER
8c. ADDRESS (City, State, and ZIP Code)	10. SOURCE OF FUNDING NUMBERS PROGRAM ELEMENT NO. / PROJECT NO. / TASK NO. / WORK UNIT ACCESSION NO.
11. TITLE (Include Security Classification) See Box 19	
12. PERSONAL AUTHOR(S) Christina N. Walton, B.S., 2d Lt, USAF	
13a. TYPE OF REPORT MS Thesis 13b. TIME COVERED FROM _____ TO _____ 14. DATE OF REPORT (Year, Month, Day) 1987 December 15. PAGE COUNT 111	
16. SUPPLEMENTARY NOTATION	
17. COSATI CODES FIELD / GROUP / SUB-GROUP	18. SUBJECT TERMS (Continue on reverse if necessary and identify by block number) Multiple apertures, field-of-view, thin lens, off-axis, aberrations, beam degradation.

19. ABSTRACT (Continue on reverse if necessary and identify by block number)

TITLE: ABERRATIONS: THEIR EFFECT ON OFF-AXIS BEAM STEERING

Thesis Chairman: James P. Mills, Lt Colonel, USAF
Assistant Professor of Physics

Approved for public release: IAW AFR 190-1.
LYNN E. WOLAVER
Dean for Research and Professional Development
Air Force Institute of Technology (AFIT)
Wright-Patterson AFB OH 45433

20. DISTRIBUTION/AVAILABILITY OF ABSTRACT ☐ UNCLASSIFIED/UNLIMITED ☒ SAME AS RPT. ☐ DTIC USERS	21. ABSTRACT SECURITY CLASSIFICATION UNCLASSIFIED
22a. NAME OF RESPONSIBLE INDIVIDUAL James P. Mills, LtCol, USAF	22b. TELEPHONE (Include Area Code) (513) 255-4498 22c. OFFICE SYMBOL AFIT/ENP

DD Form 1473, JUN 86 — Previous editions are obsolete. — SECURITY CLASSIFICATION OF THIS PAGE

BLOCK 19: ABSTRACT

The effect of aberrations on off-axis beam steering for multi-aperture systems was qualitiatively investigated. A new expression analogous to Goodman's Thin Lens is proposed which shows beam degradation that occurs at angles, with respect to the optic axis, much greater than five degrees for a thin lens, and two degrees for a thick lens. This expression was then applied to three multi-aperture configurations as a way to correctly predict the field-of-view for various optical systems. Analytical predictions supported by computational and experimental results are included. Although the beam degradation as the field-of-view or field angle is increased has a dramatic effect on the image quality, the power loss as the field angle is increased will be the major factor in the design for a system of this type.